FEDERAL UNIVERSITY OF ESPÍRITO SANTO
TECHNOLOGICAL CENTER
GRADUATE PROGRAM IN ELECTRICAL ENGINEERING

Master's Dissertation

Equivalent Grid-Following Inverter-Based Generator Model for ATP/ATPDraw Fast Time-Domain Simulations

Matheus Bassani Luchini

VITÓRIA – ES

JULY/2023

Matheus Bassani Luchini

Equivalent Grid-Following Inverter-Based Generator Model for ATP/ATPDraw Fast Time-Domain Simulations

Dissertation presented to the Graduate Program in Electrical Engineering from the Technological Center of the Federal University of Espírito Santo as a partial requirement for obtaining a Master's Degree in Electrical Engineering.

Supervisor: Prof. D. Sc. Oureste Elias Batista
Co-supervisor: Prof. D. Sc. Felipe Vigolvino Lopes

VITÓRIA – ES

JULY/2023

Ficha catalográfica disponibilizada pelo Sistema Integrado de
Bibliotecas - SIBI/UFES e elaborada pelo autor

Luchini, Matheus Bassani, 1996-
L936e Equivalent grid-following inverter-based generator model for ATP/ATPDraw fast time-domain simulations / Matheus Bassani Luchini. - 2023.
67 f. : il.

Orientador: Oureste Elias Batista.
Coorientador: Felipe Vigolvino Lopes.
Dissertação (Mestrado em Engenharia Elétrica) - Universidade Federal do Espírito Santo, Centro Tecnológico.

1. Sistemas de energia elétrica. 2. Energia - Fontes alternativas. 3. Curtos-circuitos. 4. Modelos e construção de modelos. 5. ATP (Programa de computador). I. Elias Batista, Oureste. II. Vigolvino Lopes, Felipe. III. Universidade Federal do Espírito Santo. Centro Tecnológico. IV. Título.

CDU: 621.3

Matheus Bassani Luchini

Equivalent Grid-Following Inverter-Based Generator Model for ATP/ATPDraw Fast Time-Domain Simulations

Dissertation presented to the Graduate Program in Electrical Engineering from the Technological Center of the Federal University of Espírito Santo as a partial requirement for obtaining a Master's Degree in Electrical Engineering.

Approved in july 24th of 2023

EXAMINING COMITTEE:

Prof. D. Sc. Oureste Elias Batista
Federal University of Espírito Santo
Advisor

Prof. D. Sc. Felipe Vigolvino Lopes
Federal University of Paraíba
Co-advisor

Prof. D. Sc. Lucas Frizera Encarnação
Federal University of Espírito Santo
Internal Examiner

Prof. D. Sc. Mário Oleskovicz
University of São Paulo
External Examiner

To my parents, for being unconditionally by my side.

Acknowledgements

First of all, I thank God for blessing me in every moment of my life. Thanks to my parents for being my examples and for always being by my side. You are the reason to all my effort and dedication. Without you, it would have been impossible to get where I am today. I also thank my family for supporting, cheering and believing in me, understanding my absence in some moments.

I thank my friends for the many moments we shared, whether they are good or bad. Having you with me made this journey so much more meaningful and lighter. You are a part my life and I will carry you with me forever in my heart. A special thanks to Larissa Grassi and Vinicius da Luz, with whom I shared more closely these two years. Your technical and, above all, emotional support were fundamental for us to reach the end of this professional chapter.

I would like to thank my advisors, Prof. D.Sc. Oureste Batista and Prof. D.Sc. Felipe Lopes for accepting the challenge of guiding me during this Master's Program and for always showing me a way, even when it didn't seem to exist. I will be eternally grateful for the availability, even in such a different and challenging format when most of the time it was not possible for us to be together physically. I will carry all the teachings with me forever.

Finally, I would like to thank the Federal University of Espírito Santo for providing public, free and quality education and to all professors and employees of the Graduate Program in Electrical Engineering for contributing to my personal and professional growth. Also, I thank the Espírito Santo Research Foundation (Fapes) for the financial support.

Ah, not in knowledge is happiness, but in the acquisition of knowledge! In forever knowing, we are forever blessed; but to know all, were the curse of a fiend.
(Edgar Allan Poe)

Abstract

Due to the increasing penetration of inverter-based resources (IBR) in modern power grids, most phasor-domain models became insufficient to represent the system dynamics during steady-state and fault conditions. As a result, IBR time-domain models gained importance. However, complete models that include switching elements and their respective controllers are usually time-consuming and difficult to initialize, especially in systems with several IBRs connected. Thus, this work presents an equivalent time-domain grid-following inverter-based generator (IBG) model, which can be used in Electromagnetic Transients Programs (EMTP). The proposed IBG model is developed in the Alternative Transients Program (ATP) using the ATPDraw graphical interface. A complete benchmark photovoltaic model available in ATP/ATPDraw environment is taken as reference to evaluate the proposed equivalent IBG model under steady-state and fault scenarios. The obtained results showed that the proposed model is simpler and less time-consuming than the complete model, being capable of easily considering the implementation of different components/controls of IBR in EMTP. The settings used in the implemented control schemes proved to be effective, resulting in an average error of about 2.21% during fault conditions. Also, a reduction of about 70 % in the execution time was achieved when compared to the analyzed benchmark one, attesting its usefulness for power system studies with high presence of grid-following IBRs.

Keywords: ATP. EMTP. electromagnetic transients. grid faults. IBR. time-domain modeling.

Resumo

Devido à crescente penetração de fontes que se conectam à rede por meio de inversores (IBR, do inglês inverter-based resources) nos sistemas elétricos de potência atuais, a maioria dos modelos no domínio fasorial se tornaram insuficientes para representar às dinâmicas do sistema em regime permante e durante faltas. Como resultado, modelos no domínio do tempo ganharam importância. No entanto, modelos completos que incluem elementos chaveados e seus respectivos controles geralmente apresentam elevado custo computacional e dificuldades de inicialização, em especial em sistemas com muitos IBRs conectados. Dessa forma, este trabalho apresenta um modelo equivalente no domínio do tempo de gerador baseado em inversor seguidor de rede que pode ser usado em Electromagnetic Transients Programs (EMTP). O modelo proposto foi desenvolvido no Alternative Transients Program (ATP) usando a interface gráfica ATPDraw. Um modelo de gerador fotovoltaico chaveado disponível no ATP/ATPDraw foi usado como referência para avaliar o desempenho do modelo proposto em regime permanente e durante a ocorrencia de faltas. Os resultados obtidos mostraram que o modelo proposto é mais simples e apresenta menor custo computacional que o modelo completo, sendo capaz de facilmente considerar diferentes controles e componentes internos. Os ajustes e controle utilizados mostraram-se efetivos, resultando em um erro médio de 2.21% nos cenários de falta. Além disso, uma redução de 70% no tempo de execução foi alcançado quando comparado com o modelo de referência, atestando assim seu valor para estudos de sistemas elétricos de potência com elevada penetração de IBRs seguidores de rede.

Palavras-chave: ATP. EMTP. transitórios eletromagnéticos. faltas na rede. IBR. modelagem no domínio do tempo.

List of Figures

List of Tables

List of abbreviations and acronyms

A	Ampere
AC	Alternating Current
ATP	Alternative Transient Program
DC	Direct Current
DSOGI	Decoupled Second-Order Generalized Integratetor
EIBR	Equivalent Inverter-Based Resource
EMTP	Electromagnetic Transients Program
Hz	Hertz
IBG	Inverter-Based Generator
IBR	Inverter-Based Resources
IGBT	Insulated-Gate Bipolar Transistor
kW	kilowatt
kVA	kilovolt-ampere
kvar	kilovolt-ampere reactive
LG	Line-to-Ground
LPF	Low-Pass Filter
EPS	Electric Power Systems
GS	Grid Synchronization
P	Active Power
PC	Power Converters
PI	Proportional–Integral
PLL	Phase-Locked Loop
POC	Point of Connection
PSC	Positive-Sequence Calculator

PV	Photovoltaic
PWM	Pulse Width Modulation
Q	Reactive Power
QSG	Quadrature Signals Generator
RMSE	Root Mean Squared Error
S	Aparent Power
SG	Synchronous Generators
SRF	Synchronous Reference Frame
TACS	Transient Analysis of Control Systems
V	Volt
2L	Line-to-Line
2LG	Double Line-to-Ground Fault
3L	Three Line Fault
3LG	Three Line-to-Ground Fault

List of symbols

α	Greek letter alpha
β	Greek letter beta
e	Euler's number
E	Voltage amplitude
I_{abc}	Grid currents in *abc* referential frame
i_d	*d*-component of grid current
i_q	*q*-component of grid current
j	Imaginary unit
τ	Greek letter tal
V_{abc}	Grid voltages in *abc* referential frame
$V_{\alpha\beta}$	Grid voltage in $\alpha\beta$ referential frame
$V_{\alpha\beta}^{+}$	Positive-sequence component of grid voltage in $\alpha\beta$ referential frame
v_a	Phase A voltage
v_b	Phase B voltage
v_c	Phase C voltage
v_d	*d*-component of grid voltage
v_q	*d*-component of grid voltage
V_{abc}^{+}	Positive-sequence component of grid voltage in referential frame
k_p	Proportional gain
k_i	Integrative gain
θ	Angle
ω	Frequency

Contents

1 Introduction

The evolution of society over the years, especially after the First Industrial Revolution, significantly impacted the way various goods are generated, transported and consumed. When it comes to items such as electricity, this process is becoming more and more complex due to the increase in demand, change in consumption profile, climate changes and insertion of new elements. Therefore, it is essential the development of mechanisms to help in the analysis to and subsidize the safe, continuous and reliable operation of the systems, thus guaranteeing that the customers have their demands met and, finally, ensuring the proper functioning of other activities that depend on these goods.

When it comes to transmission and distribution energy systems, the complexity relies on the extension and topology of the networks and the use of a variety of components and different technologies. In this sense, it is of paramount importance to develop new tools to deal with electrical grids [National Academies of Sciences Engineering & Medicine, 2016].

As stated before, the climate changes are also a motivation for the aforementioned changes. Due to the growing environmental awareness, nonrenewable and highly polluting sources, as coal power plants, are giving space to renewable sources, specially solar and wind power plants, as can be observed in the graphic presented in Figure 1.

Figure 1 – Share of cumulative power capacity by technology up to 2027

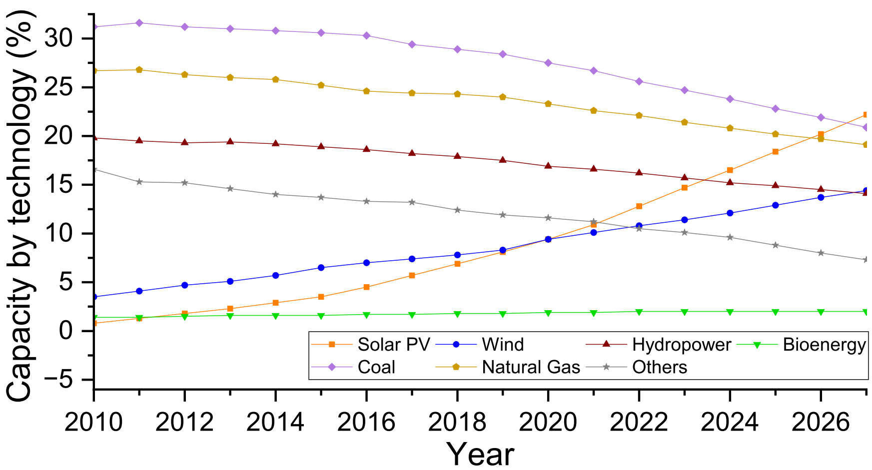

Source: Adapted from International Energy Agency [2022]

This graphic shows the participation of some sources in the world electrical matrix over the last years and a forecast for the next ones. It is clear the growth of solar and wind, evidencing that in 2027 the photovoltaic (PV) systems are expected to consolidate as the primary source of energy worldwide. Some of these generations have been widely referenced to as Inverter-Based Resources (IBRs), since their interface with the grid is based on inverters. As a result, the Electric Power Systems (EPS) will face several technical challenges, because the IBR dynamic during faults or even during some normal operation conditions does not follow the well-known behavior of synchronous generators (SG), posing difficulties on system protection and control applications [LOPES et al., 2022].

In this sense, the characteristics of present and future electrical grids are evidenced in Figure 2.

Figure 2 – Characteristics of present and future electrical grids

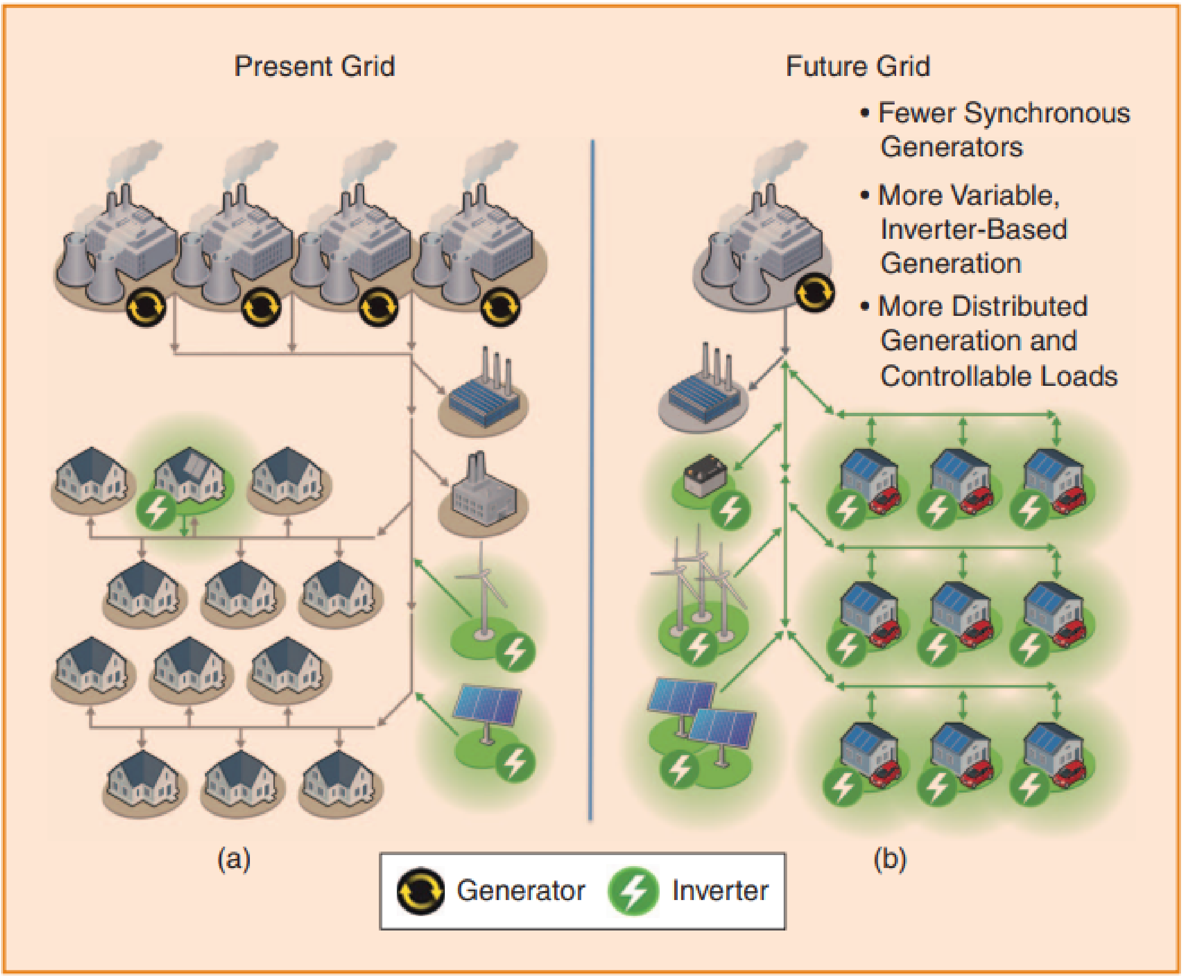

Source: Kroposki et al. [2017]

As can be seen, present grids are composed mainly by SG having large rotational inertia, as hydropower and thermal power stations. Furthermore, the generation centers are usually concentrated in large power plants located far from consumer centers, e.g. hydroelectric plants that need large reservoirs formed in the beds of a river. On the other hand, future grids will be composed by fewer SG, which will decrease the total inertia of the system. The distributed resources, with the energy being produced next to consumption, are expected to be dominant. Considering that these distributed generation are mostly PV-based, that large wind and solar power plants are are gaining space, as shown in Figure 2 and that the discussion of achieving a 100 % renewable grid is a reality, the growing number of inverter-based devices will result in an inverter-dominated grid since this technology will represent more than 50 % of the rated power at any time [KROPOSKI et al., 2017].

In this scenario, the development of simulation-based studies to understand the impacts of these new technologies is imperative, since the behavior of the EPS can change with regard to short-circuit levels, voltage and frequency control, loss of inertia (when considering PV sources), variability and uncertainty of the generators power output etc [MOHAMMED; ALHELOU; BAHRANI, 2023; National Academies of Sciences Engineering & Medicine, 2016].

Also, the operating conditions of the inverters tend to be more severe in the next years since the climate change is setting temperature records, as in July 2023 when the global air and ocean temperatures reach a new maximum value, as stated by the Copernicus Climate Change Service [2023]. Therefore, the simulation-based studies also have to investigate the impact of these sudden climate changes in the power injection of these equipment in order to validate its functioning under these conditions and also evaluate the operation of IBRs in general considering the mentioned changes.

Historically, most power flow and short-circuit simulation tools have been developed for steady-state evaluations in phasor-domain. Although these models allow the representation of most important features of traditional synchronous power systems, limitations have been found to emulate the dynamic behavior of IBRs [CORPORATION, 2017], especially when faults or any other disturbances take place. Hence, detailed full models have been proposed for time-domain simulations, leading Electromagnetic Transients Program (EMTP) to gain importance in the context of IBR studies. However, as reported in Mendes et al. [2019] and Hassani et al. [2022], although full time-domain IBR models are realistic, they emulate switching components and their respective control schemes, resulting in complex and time/computational-consuming simulations. It has motivated developments in power system modeling area to obtain simplified, but representative IBR models.

The equivalent IBR models available in the literature are often phasor-based and consider only steady-state response [MENDES et al., 2019; HWANG et al., 2016; POLAJžER et al., 2021]. This limits pre-operational and operational time-domain studies, since possible impacts of IBRs are not adequately emulated during transient events. Dynamic models can be found in the literature. However, they often disregard faulty conditions [QUEIROZ; MENDES; BATISTA, 2021] or do not make comparisons in EMTP platforms for a better parameter adjustment, as reported in Ramasubramanian et al.

[2017]. Moreover, the mentioned models are developed in computational programs which require paid licenses, and their implementation details are not fully provided, leading potential model users to face difficulties in reproducing the IBR models and their results. There are exceptions, as in Lopes et al. [2022], in which a relevant detailed implementation of a simplified controllable source in ATP is presented. The model allows to adjust the active and reactive power, being adequate to perform power flow studies in steady-state conditions. However, in general, the lack of information about the implementation and of explanations about ways to adapt the models to different scenarios is another limiting factor, especially when one desires to test different control strategies. In addition, some works do not even mention concerns about the computational burden of the simulations, which is becoming an important aspect as the penetration of IBRs in existing systems increase.

Although the changes in EPS have motivated the development of new technologies and control strategies for the IBRs, the majority of inverters currently use the grid parameters, e.g. voltage amplitude and frequency, to which they are connected as a reference for the operation of the equipment and thus for the power injection [MOHAMMED; ALHELOU; BAHRANI, 2023], which will be explained in detail in the next sections. Because of these characteristics, these inverters are called grid-following and are the most adopted in the simulations for EPS studies.

Considering the above-mentioned context, this work proposes an equivalent grid-following IBR model for EMTP, which is developed in ATP/ATPDraw environment. The model is able to represent the dynamic of IBRs during steady-state and under balanced and unbalanced fault conditions, allowing the representation of different power injection dynamics. A straightforward implementation in ATP/ATPDraw (which can be expanded for other EMTP) with computational burden lower than those of full EMTP IBR models is achieved. The proposed model software implementation is detailed, providing to experienced and beginning ATP/ATPDraw users a reference guide to simulate equivalent IBR models. For validation purposes, a benchmark grid-following PV power plant model available in ATP/ATPDraw is taken as reference. The obtained results show that the proposed model properly represents the IBR operation, revealing that the implementation methodology facilitate the adoption of different control strategies or model components.

1.1 Problem Statement and Objectives

1.1.1 Problem Statement

The research problem to be addressed in this Dissertation is: how to implement an equivalent grid-following inverter-based generator model for fast time-domain simulations that is capable of representing system dynamics during steady-state and faulty conditions using ATP/ATPDraw?

1.1.2 Dissertation Objectives

1.1.2.1 General objective

This dissertation aims on developing an equivalent inverter-based generator model that can be used in time domain simulations with smaller computational cost when compared to complete switched models.

1.1.2.2 Specific objectives

The specific objectives of this dissertation are listed below:

- Develop an equivalent inverter-based generator model in ATP/ATPDraw;
- Investigate the model's behavior during steady-state and under distorted conditions, as balanced and unbalanced faults;
- Detail the software implementation of the proposed model;
- Serve as a reference guide for those who uses ATP/ATPDraw in EPS analysis; and
- Allow the user to easily change control schemes or IBR internal components by maintaining the internal variables explicit.

1.2 Motivation

The understanding of the structure and components of the electric power systems is fundamental in order to assure it reliable and safe operation. Moreover, it is know that these systems are undergoing profound changes in their configuration and components. This said, the motivation for this work is based on the necessity to develop tools capable of help in understanding the impacts brought by these changes, in this specific case, the advancement in the use of inverters to interface energy sources with the EPS. In this context, the model proposed here can be used to face these new challenges when applied in analyses that aim to identify these impacts, ensuring that it is possible to keep chasing more technological and reliable electrical grids while the use of renewable sources continues to increase.

In addition, it is also a motivation the use of ATP/ATPDraw to implement the proposed model since this software is gaining more and more notoriety among researchers all over the world concerning EPS studies. Moreover, although the Federal University of Espírito Santo (Ufes) group study in this topic has several developments and published works providing simpler models for steady-state analysis or without considering grid faults and using other platforms, the use of ATP/ATPDraw is a important step to expand research horizons and contribute to the creation of partnerships with universities and research centers throughout Brazil and abroad. Following this path, this work emerged as a partnership to continue the work developed in Lopes et al. [2022].

1.3 Publications

The results of this research were synthesized in a paper, entitled "Equivalent Grid-Following Inverter-Based Generator Model for ATP/ATPDraw Simulations", that was presented at the 2023 International Conference on Power Systems Transients (IPST) on 12 June 2023 in Thessaloniki, Greece. The paper is also part of a Special Issue of the Electric Power Systems Research journal of Elsevier in which papers from IPST will be made available. DOI: 10.1016/j.epsr.2023.109624.

1.4 Dissertation Structure

This section introduces the subject of this dissertation and presents its objectives and motivation. In Chapter 2 a theoretical background dealing with the topics that are necessary to completely understand the proposed model are given. In Chapter 3, readers find details of the software implementation with the structures, parameters and control strategies adopted. Chapter 4 presents and discusses the simulation's results. In Chapter 5, the conclusions are presented and future works are considered. The references are listed at the end of this dissertation.

2 Theoretical Background

In this chapter, the foundation on grid-following inverters and its modeling, which play a crucial role in integrating renewable energy sources into the electrical grid, is presented. An insightful literature review is summarized in order to comprehensively understanding the fundamental principles that govern the behavior of these elements, their control strategies, operational limitations identify and to identify gaps in current knowledge and establish the rationale for the contributions of this research. Also, the necessary knowledge about the faults that occur in the EPS are provided, as well as information about the software used to implement the model and carry out the simulations.

2.1 Inverter-based resources

Historically, electric power systems are dominated by traditional synchronous generation since hydropower, coal, nuclear, and gas systems, the main sources of electricity worldwide, connect to the grid through SG. In recent years, however, the advance of new sources has changed this structure. The advance of wind and solar power plants, for example, bring with them an increasing penetration of power converters (PC) since there are sources in which the interface with the electrical grid are done by using inverters [MOHAMMED; ALHELOU; BAHRANI, 2023].

Depending on the operational characteristics of the PC used to interface the IBR with the electrical grid, they can be classified into three main categories, namely: grid-forming, grid-following and grid-supporting [ROCABERT et al., 2012]. A basic representation of each type is illustrated in Figure 3, considering that the grid-supporting usually have two implementation possibilities.

In this work, the grid-following (or grid-feeding), presented in a simplified way in Figure 3(a), was chose to deliver the generated power (P for active power and Q for reactive power) to an existing electrical grid. It must be highlighted that, as a grid-following, this type of PC utilizes the characteristics of the grid to which it is connected, i.e., the current source must be properly synchronized with the voltage at the connection point, being the phase-locked loop (PLL) a typical approach for this task. In this way, it is guaranteed the accurate exchange of active and reactive powers. Since a formed grid is mandatory for the operation of this converter, it cannot be used in island mode. Most of the distributed generation systems (like in photovoltaic or wind power systems, for example) employ this technology nowadays [BIALASIEWICZ, 2008]. In fact, PC were limited to grid-following control strategy in the last years. However, the changes in the EPS led to the emergence of new strategies in order to meet the new requirements of these networks [MOHAMMED;

Figure 3 – Representation of grid-connected power converter main types

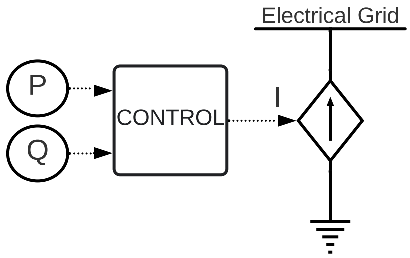

(a) Grid-following

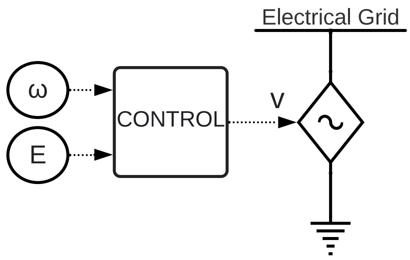

(b) Grid-forming

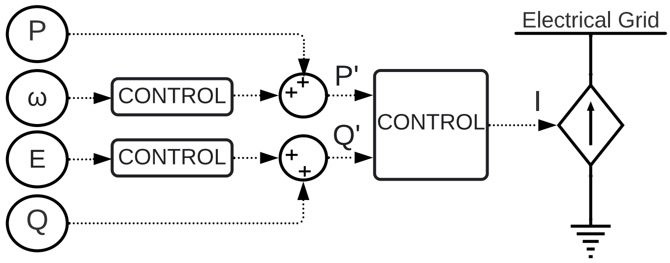

(c) Grid-supporting based on current-source

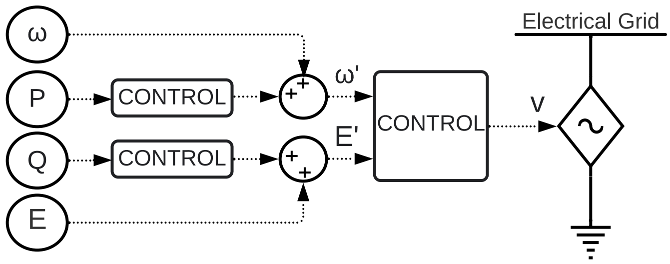

(d) Grid-supporting based on voltage-source

Source: Adapted from Rocabert et al. [2012]

ALHELOU; BAHRANI, 2023].

When the operation in island mode is required, for example, a grid-forming control technique can be used. It can be represented by an ideal voltage source, as can be seen in Figure 3(b). This type of PC is able to set the voltage amplitude E and frequency ω of the grid. In case of a grid failure, the voltage imposed by the grid-forming can be used as reference for other grid-feeding connected to the system.

Between these two, the grid-supporting can be found. This group is composed by two main types of PC: current-source-based grid-supporting and voltage-source-based grid-supporting, as shown in Figures 3(c) and 3(d), respectively. With these types of PC, the adopted control scheme allows to contribute to the regulation of grid parameters, namely voltage amplitude E and frequency ω by delivering proper values of active and reactive power [VASQUEZ et al., 2009], contributing, for example, to improve power quality [REICHERT; GRIEPENTROG; STICKAN, 2017]. When implemented based on current-source, the PC is not capable of operating without at least one grid former, which might lead to a discussion of the differences for the grid-following. Although this answer still has gaps since the grid-supporting is an emerging technology, the differences are major related to the objective of regulating grid parameters by controlling the power injected. In turn, the implementation based on a voltage-source can operate in both grid-connected and island mode.

2.2 Review on IBR models

It is possible to find several full time-domain IBR models in EMTP platforms. However, most of them require complex and time-consuming simulations [HASSANI et al., 2022]. To overcome this situation, simplified IBR average models have been also reported, but usually they cannot emulate the IBR response under fault conditions [CORPORATION, 2017]. Basically, full time-domain IBR models include the source (often photovoltaic or wind generators, with maximum power point tracking), power converters with their associated controls, and AC filters at the connection point to the grid. As this type of model simulates the system at the switching level [ROPP; GONZALEZ, 2009], high simulation times are required in order to obtain accurate results since very small time steps need to be used in EMTPs [SEUSS et al., 2017].

A dynamic three-phase single-stage grid-connected PV model is proposed in [DASH; KAZERANI, 2011]. Current-source inverters built via reverse-blocking IGBT switches are used to do so. The control of the DC-side current and the current injected into the grid are performed, respectively, by an outer and an inner current control loops. Changes in the irradiance level and faulty conditions are analyzed, with the results remaining consistent. However, the primary source of energy is limited to PV systems, since the flexibility to modify this component is not discussed. In addition, a three-phase space vector controlled voltage source inverter is proposed in Dongdong et al. [2019]. The simulations are built in Matlab/Simulink environment, and only voltage and current waveforms are presented, such that guidelines to reproduce the model in detail are not presented.

In Nanou e Papathanassiou [2014], a switching-level model is presented. The reference voltage for a PV array is provided by a control consisting of a PI compensator in the DC-side. The AC-side control is based on cascaded two-level current regulators with a proportional-resonant compensator, which acts on the inverter output current regulation.

To assist the electrical grid during a fault condition, the control scheme is modified to provide reactive current. This complete model was used as reference to develop a simplified version, which consists of a fundamental frequency one that adds to the signals high-frequency content related to the switching process. Aiming to reduce the model complexity and associated computational burden, switches are replaced by mathematical functions that represent their average values, and the LCL filter is replaced by an equivalent total inductance. The Matlab/Simulink platform is used to simulate the IBR model considering Synchronous Reference Frame and Decoupled Second-Order Generalized Integratetor Phase-Locked Loop units (i.e., SRF-PLL and DSOGI-PLL, respectively). Once again, details on its implementation are not provided.

The simplification of IBR models have also been proposed in several works, normally by considering only its steady-state phasor response over the time. In Mendes et al. [2019], for instance, accurate IBR phasor-domain simulations are presented. In Hwang et al. [2016], a three-phase steady-state model of a three-wire current-controlled voltage-source converter-interfaced distributed generator is reported. In addition, Polajžer et al. [2021] presents a simplified IBR model, aiming to evaluate the impact of transmission network faults on its steady-state response. In these papers, the Matlab/Simulink platform is also used to analyze steady-state phasor responses over the time. However, steady-state phasor-based models limit pre-operational and operational studies, since they are insufficient to completely emulate the impacts of IBRs into the grid, especially under fault conditions when fault ride-through and transient stability aspects must be represented. Moreover, in these works implementation details are not completely described or computational burden aspects are not addressed.

Between the two types of implementation mentioned, intermediate dynamic models can be found in the literature as well. In Ramasubramanian et al. [2017], a positive sequence converter model is developed. It allows the use of longer time steps, reducing the computational efforts required in large-scale simulations. Although a satisfactory result is observed, no significant reduction in the execution time were obtained and implementation details are not provided. Also, a comparison with EMTP simulations in order to obtain a better parameter adjustment is not carried out, being suggested for future works by the authors.

In Queiroz, Mendes e Batista [2021], the development of simplified models in Matlab/Simulink, with lower computational burden than full models is discussed. Norton equivalents are used to represent the DC-side. The behavior of the AC-side is defined by using the power balance principle and, as a result, the injected current depends only on: power, power factor and grid voltage. To demonstrate the impacts of the high insertion of distributed generators in distribution networks (namely, IEEE 13 Node Test Feeder) is the goal in this work. However, the scope of such a reference neither include the analysis of voltages, currents, grid injected power over the time, i.e., nor consider faulty conditions, what does not meet the expectations for transient studies via EMTP. Also, detailed guidelines about the software IBR modeling are not provided, as most references, which is critical for EMTP users.

In addition to the models commented so far, one can find other works applying computational IBR models, but with other purposes than those related to modeling aspects, as considered here. For instance, in Sarmiento, Carreno e Z. [2018], the focus is on specific features of inverter, as droop control and intelligent volt-var control in grid-connected and islanded mode. The models are developed in Matlab/Simulink and compared with OpenDSS results, considering only steady-state operation. In Turner-Bandele, Pandey e Pileggi [2021], the power flow solver SUGAR is used to test the analytical distributed IBR models with current limitation and volt-var control strategies. The results are compared with measurements generated via EMTP simulations (namely, using EMTP-RV and GridLAB-D software). A voltage-modulated direct power control is analyzed in Gui et al. [2019] when a weak grid is considered. However, in none of these works, since they are not focused on IBR modeling aspects, there are implementation details which are not fully explained, posing difficulties on the reproduction of these models.

In Lopes et al. [2022], the authors present a detailed implementation of a simplified controllable source in ATP/ATPDraw which can represent electrical energy resources and loads with adjustable power (active and reactive). The results are compared with a detailed photovoltaic ATP/ATPDraw benchmark power plant model ([HOIDALEN; PRIKLER; PENALOZA, 2021]) and show that the proposed system is accurate and reliable for power flow studies when stable voltage and steady-state conditions are considered. Although the work presents all the necessary implementation details for the reproduction of the system, the fact that it was published in Portuguese limits its access by researchers around the world. Furthermore, elements are missing for the model to be able to made control variables explicit, thus allowing other implementations to be considered. This is presented as a future work in order to evolve the proposed model for short-circuit analysis, including control elements capable of reproducing the dynamic response of IBR.

From the presented literature review, it can be concluded that most reported models are implemented in Matlab/Simulink, which requires a paid license, being inaccessible to many researchers around the world. Furthermore, since software implementation guidelines are often left in second plane, unclear or incomplete explanations about the IBR modeling details represent a literature gap in this topic, especially for ATP/ATPDraw users. This makes it difficult to reproduce the proposed models and, consequently, the obtained results. Indeed, although there are IBR models available in ATP/ATPDraw, they are not trivial to properly set new operation points and to change control strategies, which is taken as a limiting factor. In this sense, developing simplified, but representative, IBR models in ATP/ATPDraw environment, providing all implementation details is a considerable contribution of this dissertation, whose developments are described in the next sections.

2.3 Fundamentals of IBR modeling

A time-domain equivalent IBR model (EIBR), capable of representing grid-following technologies in a simplified way, overcoming computational issues of full switched IBR models, is developed in this work for EMTP platforms. The ATP/ATPDraw platform, a friendly and free-license software, widely used worldwide, is chosen to implement the proposed EIBR model. The main goal is to obtain an EIBR model that is generic with respect to IBRs (being capable of representing photovoltaic, wind power and storage resources, for example), being easily adapted to emulate different control schemes, such as fault ride-through strategies and associated grid codes. The proposed EIBR model is implemented considering the grid-following power converters described in Rocabert et al. [2012], being the model overview shown in Figure 4.

As a typical grid-following technology, the output currents I_{abc} of the proposed EIBR model are synthesized by taking the grid voltages V_{abc} as reference. In this way, the model is able to deliver user-specified active power P and reactive power Q levels (see Figure 4). During steady-state operation, grid quantities are well-defined, so that I_{abc} can be synthesized in a stable way. If some abrupt change occurs in the power flow conditions, this dynamic behaviors must be considered, and the IBR outputs are generated accordingly to its control schemes. In a more critical scenario, during faults, for instance, grid voltages significantly change, so that IBR fault ride-through strategies are activated. The transition period between pre-fault and fault steady-state may lead the IBR outputs to present control actions that can affect several system monitoring algorithms (protection elements, e.g.). Hence, it is of paramount importance to emulate the IBR dynamic in order to properly represent the behavior of IBR outputs.

Considering the operation of a grid-following IBR, grid synchronization (GS) is a primary task, which leads to the employment of a Phase-Locked Loop in the proposed EIBR model. Also, as the EIBR current synthesis utilizes the grid voltages as reference, it is necessary to attenuate harmonics in the measurements taken from the grid in order to obtain I_{abc} waveforms as clean as possible, especially when grid faults are considered. The PLL used in the model is implemented in the Grid Synchronization block of Figure 4, which also includes the required reference frame transforms, as can be seen. Concerning the method implementation, two different solutions are used in this work. The first one consists in a low-pass filter (LPF) and a conventional PLL (Figure 5), as considered in the model taken as reference. This proposal is used to attest the suitability of the proposed model to the reference one.

Figure 4 – Block diagram of the proposed model.

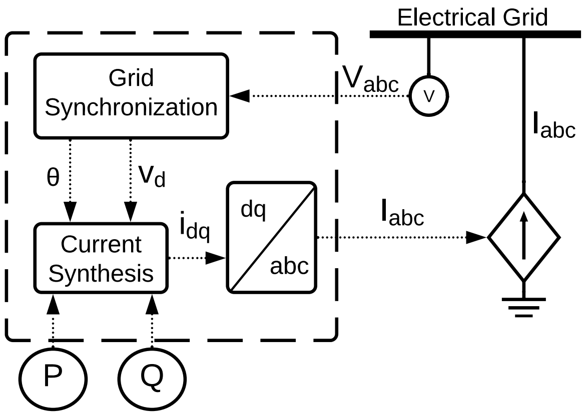

Source: Produced by the author

Figure 5 – Block diagram of the LPF and PLL.

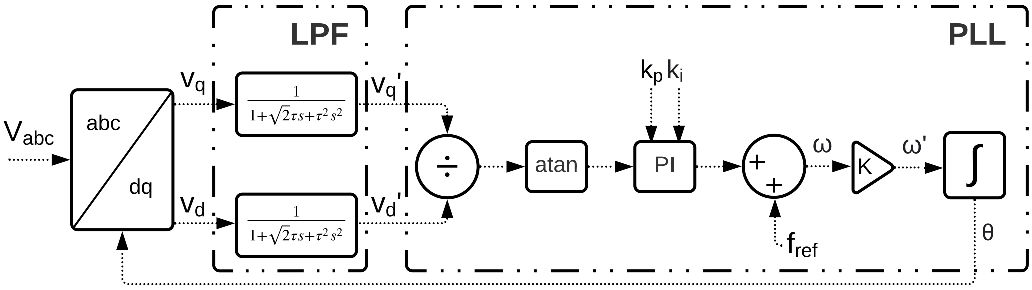

Source: Produced by the author

Although a detailed accuracy evaluation of the PLL is not among the objectives of this work, a second alternative is considered in order to assess the capacity of the proposed EIBR model to easily consider different implementations of its components. This PLL alternative adopts the DSOGI-PLL approach proposed in Kaura e Blasko [1997], as detailed in Figure 6. It provides simplicity and good response against distorted grid reference signals, resulting in a reliable frequency reference to the current synthesis process, as well as to the frequency-adaptive positive-sequence detector, which is explained later on in this section. The parameters of the proportional–integral (PI) controller in the SRF-PLL are defined according to Rodríguez et al. [2006], with minor adjustments, being $k_p = 0.8$ and $k_i = 61.69$, where k_p and k_i are the gains of the proportional and integrator controllers, respectively.

With this method, the extraction of the positive sequence fundamental component from grid voltages V_{abc} by using instantaneous symmetrical components (ISC), as reported in Arindam e Avinash [2002], results in filtered signals. By applying the symmetrical components method to the time-domain [VINTON, 1937], the instantaneous positive-sequence component V_{abc}^{+} can be obtained by means of (2.1), where $V_{abc} = [v_a \ v_b \ v_c]^T$ is

Figure 6 – Block diagram of the DSOGI-PLL.

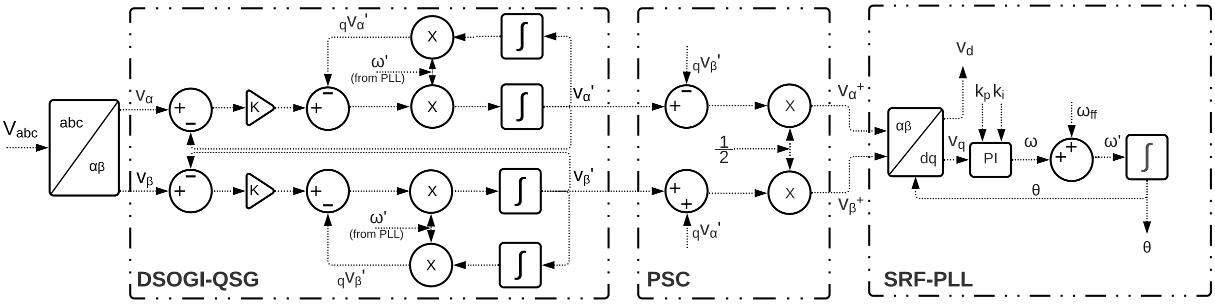

Source: Produced by the author

the grid three-phase voltage vector [RODRíGUEZ et al., 2006].

$$V_{abc}^{+} = AV_{abc}, \tag{2.1}$$

where:

$$A = \frac{1}{3}\begin{bmatrix} 1 & a^2 & a \\ a & 1 & a^2 \\ a^2 & a & 1 \end{bmatrix}, \text{ being } a = e^{-j\frac{2\pi}{3}}. \tag{2.2}$$

As said, this alternative utilizes the $\alpha\beta$ reference frame, so the use of Clarke's transformation (T_{Clark}) allows obtaining the same result of Equation (2.3), but translated to the $\alpha\beta$ stationary reference frame, with q being responsible for shifting the phase in 90° lagged to obtain the quadrature-phase waveform.

$$\begin{aligned} V_{\alpha\beta}^{+} = [T_{Clark}]V_{abc}^{+} = [T_{Clark}]AV_{abc} = \\ [T_{Clark}]A[T_{Clark}]^{-1}V_{\alpha\beta} = \\ \frac{1}{2}\begin{bmatrix} 1 & -q \\ q & 1 \end{bmatrix} V_{\alpha\beta}, q = e^{-j\frac{\pi}{2}}, \end{aligned} \tag{2.3}$$

Moreover, frequency variations are expected to take place since this work proposes the analysis of the grid behavior under fault conditions. Therefore, adaptations in the positive-sequence calculator (PSC) were required.

The need to make the PSC frequency-adaptative is the main required adaptation, what is achieved by using the DSOGI-based quadrature signals generator (DSOGI-QSG) proposed by Rodríguez et al. [2006] in combination with the SRF-PLL. A filtered version of voltages in the $\alpha\beta$ reference frame is provided by the DSOGI-QSG, which are then used as inputs in the PSC function, which is in turn responsible to extract the positive sequence component from grid voltages. Implementation details in ATP/ATPDraw of all the solutions applied in the model are addressed in the next sections.

Figures 7 and 8 show, respectively, the results of this implementation for steady state and during a voltage sag due to a grid fault. The $\alpha\beta$ phasors at the inputs of the SOGI-QSG and also its instantaneous positive-sequence component at the output of the PSC are presented.

Figure 7 – Phase and positive-sequence components in $\alpha\beta$ referential frame in steady state

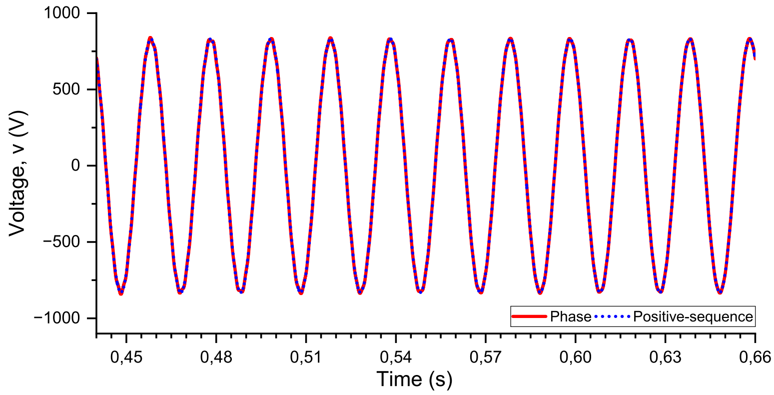

(a) Alpha

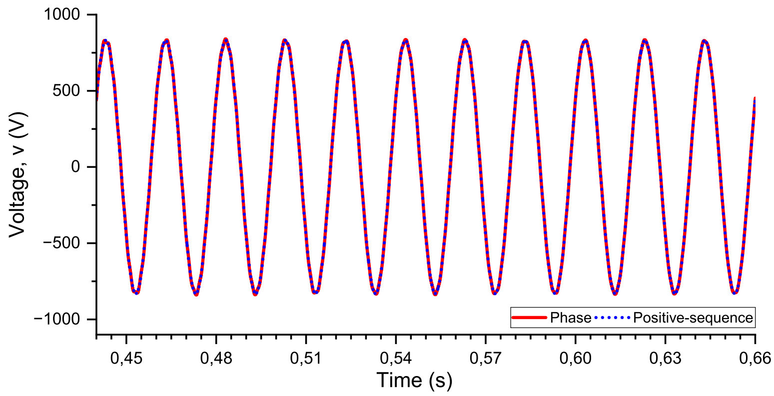

(b) Beta

Source: Produced by the author

As shown in Figure 7, the phase and positive-sequence are very similar since in steady state there isn't a significant distortion in the waveforms. In Figure 8, however, it is clear the ability of the implemented solution to filtrate the voltage signal in $\alpha\beta$ referential frame during a voltage sag.

Finally, the block responsible for synthesizing the EIBR output currents is the last component of the model. From the instantaneous power theory, P and Q can be obtained in dq synchronous reference frame as [HUANG et al., 2013]:

$$P = \frac{3}{2}(v_d i_d + v_q i_q), \tag{2.4}$$

Figure 8 – Phase and positive-sequence components in $\alpha\beta$ referential frame during a voltage sag

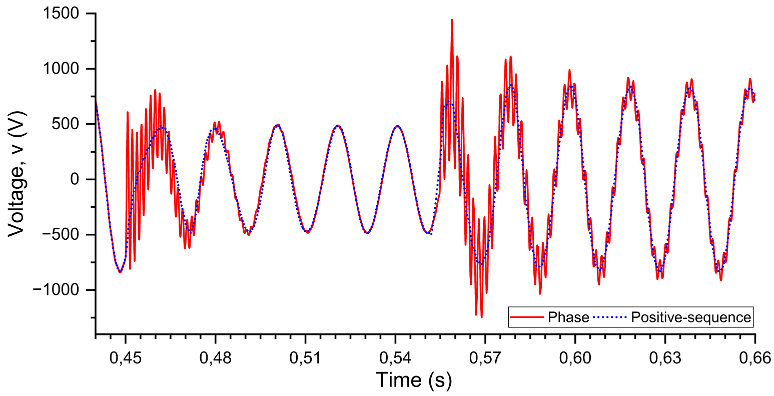

(a) Alpha

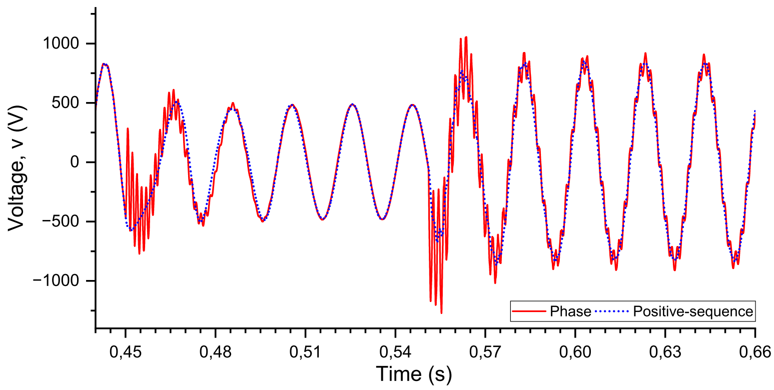

(b) Beta

Source: Produced by the author

$$Q = \frac{3}{2}(v_q i_d - v_d i_q). \tag{2.5}$$

Rearranging equations (2.4) and (2.5) and taking as reference $v_q = 0$ (since the rotating reference frame is synchronized with the grid voltage [SUYATA; PO-NGAM, 2014]), one can obtain i_d and i_q currents on the dq reference frame as functions of P, Q and voltage v_d (in turn obtained from grid voltages):

$$i_d = \frac{2P}{3v_d}, \tag{2.6}$$

$$i_q = -\frac{2Q}{3v_d}. \tag{2.7}$$

I_{abc} currents are then synthesized by performing a dq to abc transform. Due to the process explained above, these currents are synchronized with the grid and can be directly injected into the interconnected power network. Here, it is important to mention that the inverter switching components are intentionally not represented, without loss of representativeness from the grid side. Thus, I_{abc} can easily be controlled by means of different control schemes, since the strategies usually act on dq frame quantities (for instance i_d and i_q or v_d and v_q), which are explicit variables in the proposed EIBR model.

2.4 Grid faults

Electric power systems are designed to operate uninterruptedly, ensuring the quality and reliability of the delivered energy. However, they are subject to faults, from multiples causes, that can occur anytime and anywhere. These faults can be temporary or permanent and understand them, including their impacts on the system, is of paramount importance in order to assure the correct operation of the network by itself, but also of the specifics equipment that compose it.

Between several types of faults, the short-circuit are among the most common. They can have internal or external cause and represent a big risk to all equipment and people involved in the process. Concerning the duration of the event, they can be temporary or permanent. In the first case, the actuation of the protection elements is able to restore the system within a certain time without external intervention. In the case of permanent faults, however, the operator has to repair the problem in order to enable the reestablishment of the system.

The main types of short-circuit are: line-to-ground (LG), line-to-line fault (2L), double line-to-ground fault (2LG), three line fault (3L) and three line-to-ground fault (3LG). The average incidence of each type in the EPS as a whole is presented in Table 1 and a simplified representation of the electrical equivalent is shown in Figure 9.

Table 1 – Average incidence of grid fault types.

Type	Average incidence [%]
LG	70
2L	15
2LG	10
3L/3LG	5

Source: Sato e Freitas [2014].

Although the three-phase faults occur less frequently, they result in the most severe impact to the EPS. On the other hand, the most common faults (line-to-ground) are the least severe [SATO; FREITAS, 2014].

Figure 9 – Types of grid faults

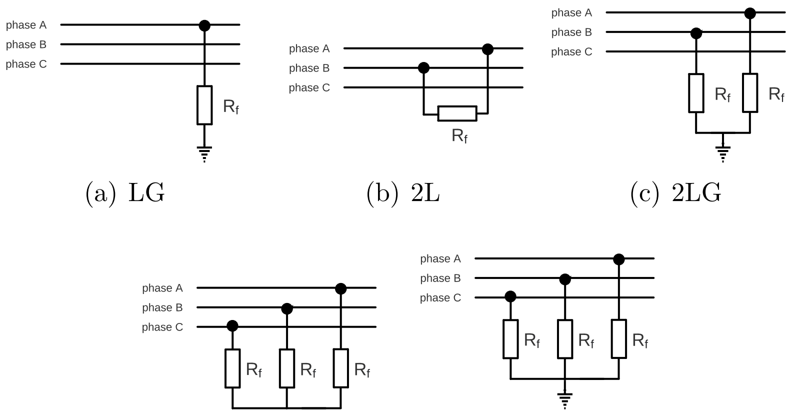

(a) LG (b) 2L (c) 2LG

(d) 3L (e) 3LG

Source: Produced by the author

2.5 ATP/ATPDraw

Computational tools are indispensable in order to analyze pre-operational and operational studies in power systems by assessing different scenarios without any physical intervention, thus assuring a reliable and safe behavior of these electrical grids. There are many software specialized (or with a package that implements electrical components), e.g. PSCAD, PTW (PowerTools for Windows), PS Simul (Power System Simulator), Matlab etc. However, they require a user license whose acquisition may be unfeasible for students and researchers worldwide.

This said, the Alternative Transients Program (ATP) appears as an open-source version of the Electromagnetic Transients Program, which is widely used for electromagnetic transients analyses. However, its applications has also included power flow and other power systems analysis [LONG et al., 1990; LOPES et al., 2022; GIMENES et al., 2022].

ATPDraw is a graphical and mouse-driven preprocessor to the ATP. The software standard Windows layout is shown in Figure 10. It offers a intuitive construction of complex networks and control systems of arbitrary structure to be simulated by using standard components. More details can be found in Hoidalen, Prikler e Penaloza [2021] and some information about the main electrical components and tools will be presented in the next sections, as well as some information about the operating principles of ATP.

2.5.1 Operating principles

ATP adopts trapezoidal integration rule in order so solve the differential equations of system components in time domain, since its predict variables of the electric power networks as function of time. Initial conditions can be determined by the user for some

Figure 10 – ATPDraw Windows user interface

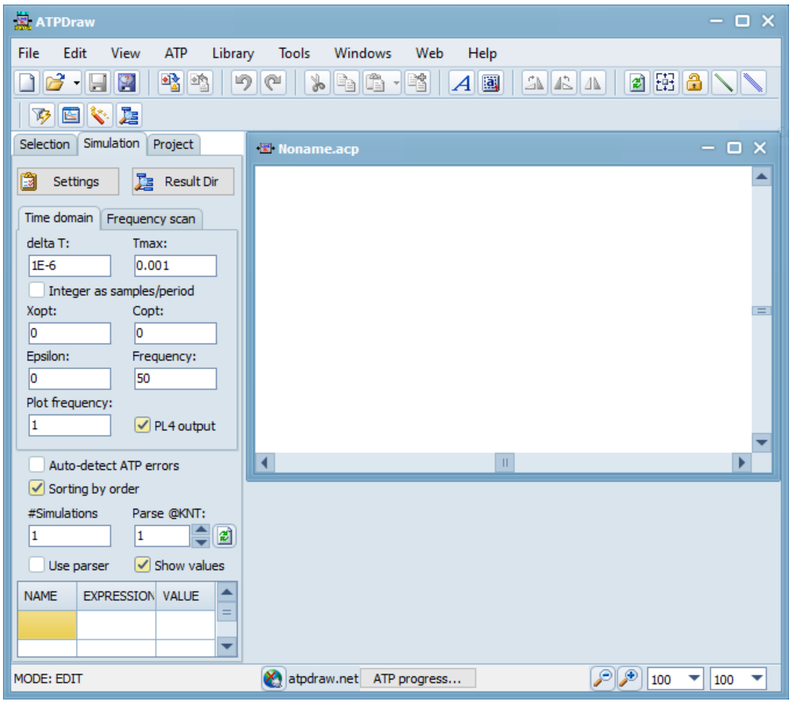

Source: Hoidalen, Prikler e Penaloza [2021]

components and also automatically by following steady-state phasor solutions.

The standard models include rotating machines, transformers, transmission lines and cables, power sources, generally with both single and 3-phase option. It is also possible to perform the simulation of symmetrical and unsymmetrical disturbances and switching operations. Control systems and components with nonlinear characteristics can also be implemented with TACS and MODELS (integrated simulation modules in ATP), which will be detailed in the next sections.

Concerning software capability, the maximum quantity of components reported for standard program distribution is show in Table 2. However, the software allows to allocate more memory in its settings, changing the mentioned limits for the desired application, if necessary.

2.5.2 MODELS

MODELS is a general-purpose simulation language which can be used for the representation and study of time-variant systems, easily connecting other programs/models to ATP. In order to define a MODELS, a free-format and keyword-driven syntax of local context is used, as the one exemplified in Figure 11. It is a default model to present the syntax of the language. From data provided by the user (d1, d2) and two inputs (i1, i2), this code calculates two different outputs (o1, o2). All codes developed for this work in MODELS language will be presented in section 3.

Table 2 – Maximum quantity of components.

Component	Limits
Busses	6000
Branches	10000
Switches	1200
Sources	900
Nonlinear elements	2250
Synchronous machines	90

Source: Hoidalen, Prikler e Penaloza [2021].

Figure 11 – MODELS code example

```
MODEL DEFAULT
DATA d1,d2      -- Data provided by the user
INPUT i1,i2     -- Inputs from another components
OUTPUT o1,o2    -- Outputs of MODELS block
VAR o1,o2       -- Variables statement
INIT            -- Variables initialization
  o1:=0
  o2:=1
ENDINIT
EXEC               -- Beginning of code execution
  o1:=(i1-i2)*t
  o2:=sin(o1)
ENDEXEC            -- End of code execution
ENDMODEL
```

Source: produced by the author

2.5.3 TACS

The TACS (Transient Analysis of Control Systems) is a tool for time-domain simulation and analysis of control systems. The exchange of signals such as voltage at a node, current, switch status, sources, time-varying resistance etc establishes the interface between TACS elements and electrical networks.

The available default implementations includes power electronics and drives, HVDC converter controls, filters, FORTRAN statements (math, trigonometric and logic functions) etc.

3 System Description

In this chapter, a comprehensive overview of the software implementation of the proposed model is provided, serving as a detailed exposition of the design and development process, elucidating the underlying algorithms, methodologies, and simulation environment employed. A step-by-step account of its architecture is presented, starting from the mathematical formulation and moving on to the implementation in the simulation platform. Through this chapter, it is intended to offer a clear and comprehensive understanding of the model, ensuring transparency and reproducibility while demonstrating its efficacy in capturing the intricate dynamics of grid-following inverters for renewable energy integration.

3.1 Software implementation of the proposed EIBR model

ATPDraw is the graphical interface of ATP. It cannot run simulations itself, but it is useful to create functional blocks, which are then used to build an ATP card which is compiled in order to run the system simulation. It disposes of a wide library of promptly available model templates, including programming modules via MODELS language and TACS elements, as stated in section 2.5. In this way, ATPDraw was the chosen software aiming to facilitate the proposed EIBR model implementation. This section explains in details each applied functional block in order to guarantee the complete description of the proposed EIBR model, allowing readers to use this work as a reference guide for the ATPDraw EIBR implementation. Such a detailed description facilitates ATPDraw users to straightforwardly reproduce the proposed model, which can be easily adapted, as desired by the user, to consider different components and control strategies given that relevant control variables are internally available.

Figure 12 presents an overview of the proposed EIBR model and the main functional blocks are numbered to facilitate the identification in the ATP/ATPDraw libraries. The interconnected power grid will be detailed in the next section.

3.1.1 GroupDef block (1)

The GroupDef block, which consists in an ATPDraw tool capable of representing an entire sub-circuit within a single block, is the one identified with number 1 in Figure 12. In this work, the GroupDef is used to implement the two different grid synchronization solutions presented is section 2.3, which are depicted in Figures 5 and 6, being their respective ATPDraw implementations presented in Figures 13 and 14, respectively.

Figure 12 – Proposed EIBR model

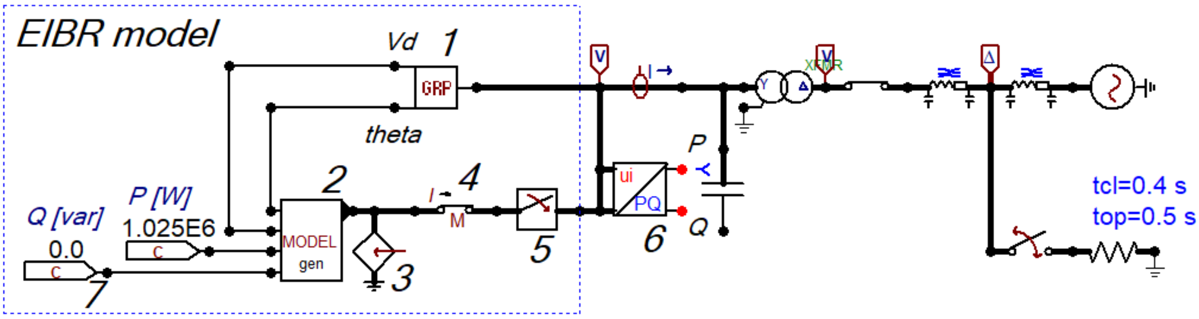

Source: Produced by the author

Before the detailed explanation of the circuits shown in Figures 13 and 14, it is necessary to present fundamental blocks that will be used in these implementations. This is done in the next subsections

Figure 13 – LPF-PLL implementation

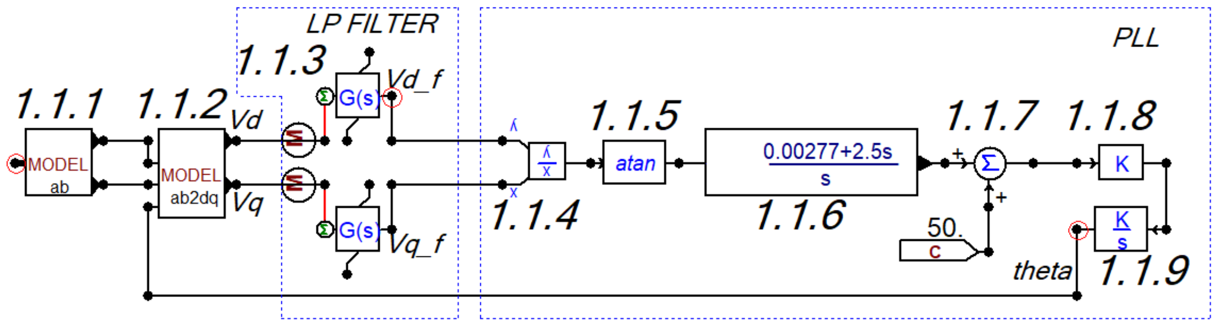

Source: Produced by the author

Figure 14 – DSOGI-PLL implementation

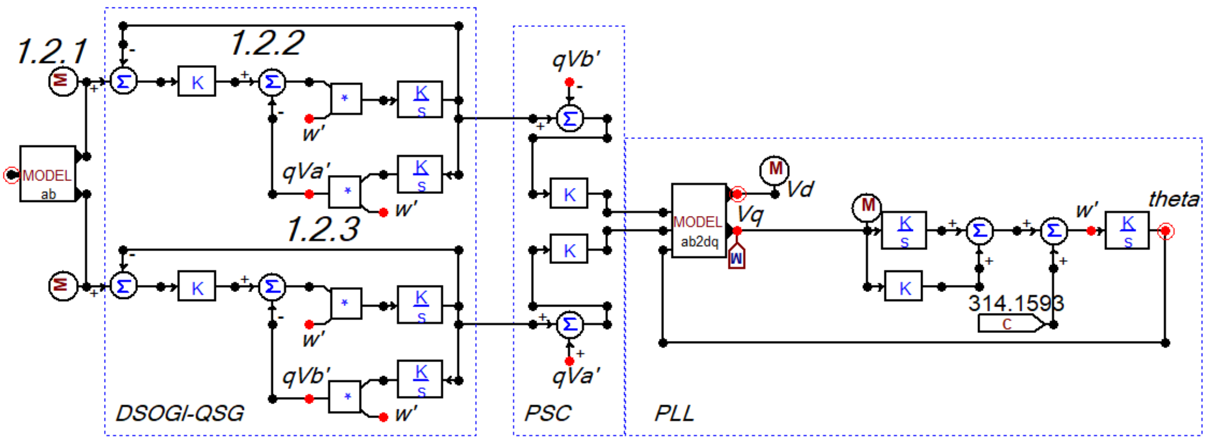

Source: Produced by the author

3.1.2 Fundamental blocks (1.1.4, 1.1.6, 1.1.7, 1.1.8, 1.2.1, 1.2.2, 1.2.3, 4, 5, 6 and 7)

Blocks that perform basic functions, such as mathematical operations, are used in many parts of the model. Blocks 1.2.2, 1.1.8, 1.2.3, 1.1.7 and 1.1.4 are TACS elements and they implement, respectively, subtraction of two input signals, multiplication by a factor of K, multiplication of two input signals, addition of two input signals and division of two input signals. No preliminary configuration is required, with the exception of block 1.1.8, in which the K factor must be set. These elements can be found in `TACS » Fortran statements » Math` tab. In addition, the block 1.2.1 is used to convert MODELS output variables to TACS class, allowing the interaction between MODELS and TACS blocks.

The block identified with number 7 is a TACS constant (`TACS » Sources » Constant`). It can be used as input in both TACS and MODELS elements. Block 4 is a measurement key available on the `Switches » Measuring` tab. It allows the ATP to recognize the current measurement point used in block 6. Thus, if power monitor block 6 is not used, block 4 becomes optional. It should be noticed that the positive relative current reference is taken in the direction from the IBR to the grid. Hence, block 6 calculates active and reactive powers values with positive and negative polarities if the EIBR model is supplying or absorbing power, respectively. To visualize the current direction reference, the output current measurement option must be activated in the key options of the block.

Still regarding block 6, it is worth mentioning that it is a native MODELS block, which is available in the `Power System Tools » PQ » PQ 3-phase` tab. As a native block, its code is available to any ATPDraw user. So, it is not detailed here. Still, some important settings are required by this block: nominal frequency (`FREQ`), sampling frequency (`SampleFreq`), as well as voltage scale (`ScaleV`), current scale (`ScaleI`) and phasor estimation method selection via `algorithm` flag (being, 0: FFT radix2-8, 1: DFT recursive or 2: alpha-beta transformation). In this work, nominal frequency and sampling rate for this block are set as 50 Hz and 400 Hz (eight samples per cycle) respectively. Also, both `ScaleV`=`ScaleI`=1 and `Algorithm`=0 are used. It should be mentioned that, for any other MODELS block, the type of the considered inputs must be configured (here, one is voltage input and the another is current input).

Finally, the use of a three-phase circuit breaker, as the one represented in block 5, at the source output is suggested. This circuit breaker can be found in the `Switches tab » Switch time 3-ph`. Although it is an optional element, its use is indicated to facilitate eventual disconnections from the grid during simulations. By using it, the need for circuit manual repositioning is avoided in cases of EIBR removal.

3.1.3 Transforms blocks (1.1.1 and 1.1.2)

The proposed EIBR model requires *abc* to $\alpha\beta$, and $\alpha\beta$ to *dq* transforms to implement its basic control scheme, as demonstrated in Figures 5 and 6. MODELS functional blocks are created from a default MODELS block to do this task. The Default MODELS block, available on `MODELS » Default model` tab, automatically adjusts (in a visual manner) inputs and outputs in ATPDraw soon after the inputs and outputs are defined in the MODELS code. Thereby, it just requires the configuration of the input types, which can be selected via double click in the block node (i.e, MODELS, TACS, voltage/current etc). Block 1.1.1 implements *abc* to $\alpha\beta$ (Clarke) transform of the grid voltage, being the associated MODELS code shown in Figure 15. The inputs of this block are the three-phase voltages of the grid, considering phase A as reference, and its outputs are the $\alpha\beta$ signals. In a similar way, the $\alpha\beta$ to *dq* transform is implemented by block 1.1.2. The inputs are $\alpha\beta$ components and the grid voltage angle extracted by means of the PLL. The block 1.1.2 MODELS code is depicted in Figure 16.

Figure 15 – MODELS code of block 1.1.1

```
MODEL ab
INPUT v[1..3]          -- Grid voltage in ABC referencial
OUTPUT alpha,beta
VAR alpha,beta         -- Variables statement
EXEC                   -- Beginning of code execution
    a := (2/3)*(v[1] - 0.5*v[2] - 0.5*v[3])
    b := (2/3)*((sqrt(3)/2)*v[2] - (sqrt(3)/2)*v[3])
ENDEXEC                -- End of code execution
ENDMODEL
```

Source: Produced by the author

Figure 16 – MODELS code of block 1.1.2

```
MODEL ab2dq
INPUT alpha,beta,theta   -- Inputs definition
OUTPUT vd,vq
VAR vd,vq                -- Variables statements
INIT                     -- Variables initialization
vd := 825
vq := 0
ENDINIT
EXEC                     -- Beginning of code execution
  vd := (a*cos(theta))+(b*sin(theta))
  vq := -(a*sin(theta))+(b*cos(theta))
ENDEXEC                  -- End of code execution
ENDMODEL
```

Source: Produced by the author

3.1.4 Grid synchronization

After the presentation of the basic and transforms blocks, the two PLL alternatives implemented with the GroupDefblock (No. 1) can be finally detailed, what will be done in the next two subsections.

3.1.4.1 Alternative 1: LPF-PLL

Considering the implementation presented in Figure 13, blocks 1.1.1 and 1.1.2 are used, as explained in the last section, to transform grid voltages into dq components. These components are then filtered by the generic transfer function block (1.1.3), available on `TACS » Transfer functions » General` tab. It is a TACS component that, in this case, implements a second order formula set according to Figure 5, with $\tau = 0.004$. The division of v_q by v_d is performed by block 1.1.4 and follows to block 1.1.5 (`TACS » Fortran statements » Trigonom » atan`), which is a TACS element that implements arctangent function. Another TACS block used, 1.1.6, represents a first order transfer function (`TACS » Transfer functions » Order 1`). Here, the gains are set as $k_p = 2.5$ and $k_i = 0.00277$, following the reference implementation [HOIDALEN; PRIKLER; PENALOZA, 2021], then forming a PI controller. Finally, the signal of the PI follows to blocks 1.1.7 (sum of two input signals), 1.1.8 (multiplication by a K constant, in this case $K = 2\pi$ and the integral block 1.1.9 in order to obtaining the grid phase estimation.

3.1.4.2 Alternative 2: DSOGI-PLL

As second PLL alternative, the DSOGI-QSG is composed by two identical circuits, which are applied to the α and β components of grid voltages. The mathematical blocks are organized to follow the scheme shown in Figure 6, being implemented by means of the already explained blocks 1.2.2, 1.1.8 and 1.2.3. Block 1.1.9 is responsible for integrating the signal. It is available in `TACS » Transfer Functions » Integral` tab, being configured with unitary gain for this application. The other required setting is the factor K in the multiplication block, being $\sqrt{2}$ the adopted gain, guaranteeing a good stabilization time and overshot limitation. The signals obtained from DSOGI-QSG follow to subtraction and addition operations in the next part of the solution, composing the PSC. The results are then multiplied a factor K (using, in this case, $K = 0.5$). Then, the positive sequence components of grid voltages in $\alpha\beta$ reference frame are obtained, being forwarded to dq transform embedded into the MODELS block and then to the SRF-PLL arrangement. Finally, a PI controller is implemented as the sum of two input signals: the integral of v_q signal (repetition of block 1.1.9, with proper K settings, which represents $k_i = 61.69$) and v_q multiplied by a constant (repetition of block 1.1.8 with K representing $k_p = 0.8$). The parameters of the PI controller in the SRF-PLL are defined according to [RODRíGUEZ et al., 2006] with minor adjustments.

3.1.5 Current synthesis and injection (2 and 3)

A relevant part of the EIBR model is the one responsible to perform the output current synthesis and injection into the grid. Blocks 2 and 3 are employed in this task. The current synthesis is carried out following equations (2.6) and (2.7), using as inputs:

the *d* component obtained from the grid voltage, which are converted into *vd*, voltage angle extracted by the PLL and the power references P and Q. It is known that, under unbalanced conditions, these equations will present some inaccuracies. However, from the errors presented later in the results (section 4), one can see that the impacts of such condition is not significant in the model considering the proposed applications. Thus, *dq* to *abc* transform is accomplished from *id* and *iq* components in order to obtain the three-phase grid currents in abc reference frame. As it can be seen in the code presented in Figure 17, this block also implements current limitation during fault conditions. The highlighted part (blue rectangle in Figure 17) represents the code part which can be modified to consider any other control strategies acting on *id* and *iq* during the current synthesis and limitation process. For example, it would allow to implement specific grid codes or inverter manufacturer specifications (as different current limitation methods, for example), evidencing the proposed EIBR model capability of being adapted to other control strategies or remodeled by using different implementation of its elements. Such a feature is facilitated due to the fact that many variables of interest are explicit, being available for manipulation in the MODELS code shown in Figure 17.

Figure 17 – MODELS code of block 2

```
MODEL GEN
INPUT vd, P, Q, theta                     -- Inputs definition
OUTPUT I[1..3]                            -- Output vector definition
VAR Id, Iq, I[1..3], Ialpha,Ibeta,Ilim    -- Variables statement
INIT                                      -- Variables initialization
  i[1..3] := 0.0
  Id := 0.0
  Iq := 0.0
  Ilim := 843.5                           -- Inom*1.02
ENDINIT
EXEC                                      -- Beginning of code execution
if t>0.02 then
    Id := P/(1.5*(vd))
    Iq := Q/(1.5*(-vd))
    Ialpha := Id*cos(theta) - Iq*sin(theta)  -- alpha beta to dq
    Ibeta := Id*sin(theta) + Iq*cos(theta)
    I[1] := Ialpha                           -- dq to abc
    I[2] := -0.5*Ialpha + (sqrt(3)/2)*Ibeta
    I[3] := -0.5*Ialpha - (sqrt(3)/2)*Ibeta
    if sqrt(Id*Id+Iq*Iq)>Ilim then           -- Current limitation
        I[1]:=I[1]*Ilim/sqrt(Id*Id+Iq*Iq)
        I[2]:=I[2]*Ilim/sqrt(Id*Id+Iq*Iq)
        I[3]:=I[3]*Ilim/sqrt(Id*Id+Iq*Iq)
    endif
else
    I[1...3] := 0
endif
ENDEXEC                                      -- End of code execution
ENDMODEL
```

Source: Produced by the author

Following with the implementation details, it is worth mentioning that since MODELS outputs in block 2 are handled internally in ATP/ATPDraw as computational variables, it is necessary to convert them into electrical currents, which is carried out via the TACS source found in `ATPDraw Sources » TACS source` tab. To ensure the correct operation of such a source, the MODELS output from block 2 is connected to the terminal of the TACS source (block 3), setting it to represent a current source. In its default form, the TACS source converts voltages, such that it has a circular shape. When “current source" option is selected, the TACs source shape changes to a diamond shape, as shown in Figure 12. It should be also noticed that the connection point of block 3 is also the beginning of the circuit that interconnects the EIBR to the grid. Hence, the synthesized currents are injected into the power network via TACS source, emulating the operation of a grid-following IBR.

3.1.6 Type of MODELS inputs and order of application adjustments

A mandatory requirement to proper implement the proposed EIBR model consists of configuring the types of inputs of the MODELS blocks. By double-clicking on each terminal of these blocks, the configuration option of the input types is given, which must be adjusted to be compatible with the source signal on each terminal. Thus, in block 1, the input must be configured as a voltage node type. In block 8, all inputs are TACS type. In block 10, the first and second inputs must be defined as MODELS type, and the others as TACS. In block 14, one input must be configured as a voltage node and the other as a current node.

Another important aspect is related to the order of application of each functional block, especially when a sequence of processes involving inputs and outputs is necessary. ATPDraw can generate ATP cards with MODELS codes in a different order than the one required, such that the user must indicate the execution sequence. Such a setting can be made in the `Order` field available in the block data window, and it can be accessed by double-clicking on the element. In the proposed model, only MODELS blocks 8 and 10 have order 1 (one), whereas the remaining ones are set with order 0 (zero).

Now, with all the above parts of the model implemented, Figures 18 and 19 aim to verify the performance of these components working together. Figure 18 illustrates the grid voltage transformed to the dq reference frame in steady-state. It should be mentioned that using dq referential frame at this point transforms control variables into DC quantities, facilitating the filtering and control process. As mentioned earlier, it is possible to verify, in Figure 18, that $v_q = 0$ due to the synchronism between the rotating reference frame and the grid voltage.

Figure 18 – Grid voltages in dq referential

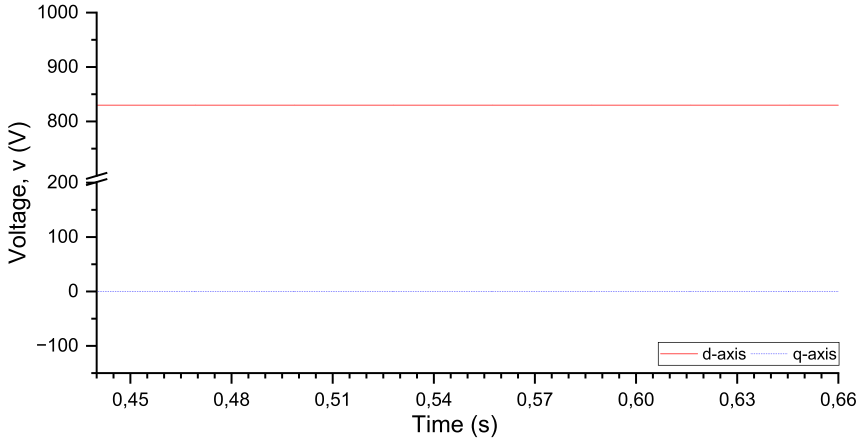

Source: Produced by the author

Finally, in order to verify the grid synchronization, Figure 19 shows grid voltage and $cos(\theta + \omega \cdot t)$ extracted from the two PLL implementations and evidences that synchronization is well established.

Figure 19 – Phase A voltage and $cos(\theta + \omega \cdot t)$ in steady-state

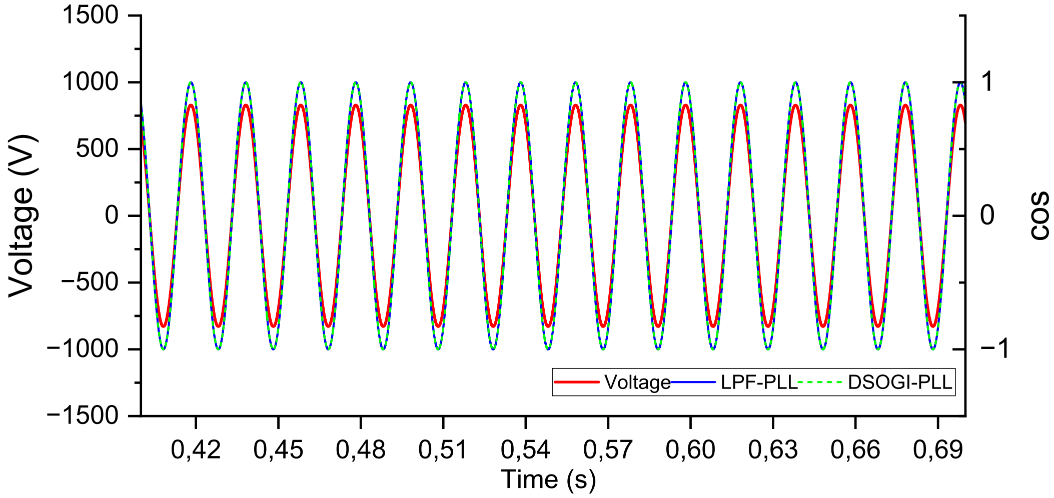

Source: Produced by the author

4 Results and Discussion

In order to validate the proposed EIBR model, two different operational conditions are assessed, namely: steady-state and during the occurrence of symmetrical and asymmetrical grid faults. The proposed EIBR model is compared with an existing ATP/ATPDraw full time-domain IBR model, which is taken as reference. This model has been built by Francisco J. Penaloza, and it is available in the ATPDraw User Manual. Such a full model simulates a PV source interfaced with IGBT PWM-controlled inverter, such as presented in Fig. 20 [HOIDALEN; PRIKLER; PENALOZA, 2021]. This model includes a PV part, the complete inverter representation, including the associated controls based on *dq* reference frame and electrical grid quantities.

Figure 20 – Original model available in ATPDraw

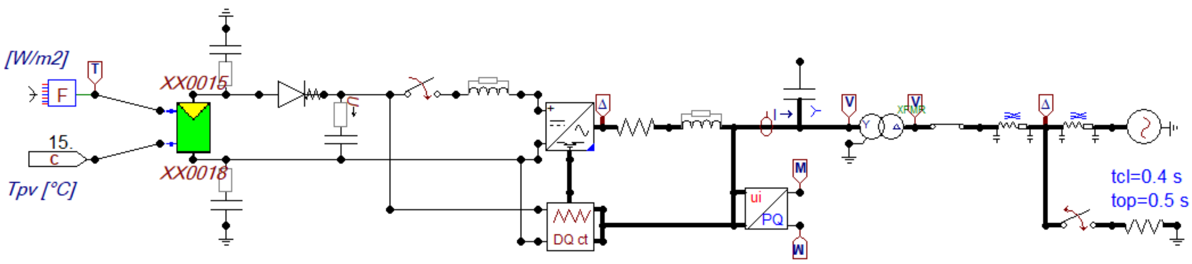

Source: [HOIDALEN; PRIKLER; PENALOZA, 2021]

The main characteristics of the grid in which the model is connected are summarized in Table 3. After the EIBR model validation, its flexibility is also evaluated by considering different grid synchronization methods and different reactive power injections.

Table 3 – Characteristics of the electrical grid adopted in the simulations.

Electrical characteristic	Adopted value
L-L voltage	22/1 kV
Frequency	50 Hz
Line R^0/R^+	2/1 Ω/m
Line L^0/L^+	40/20 mH/m
Line C^0/C^+	0.1/0.2 μF/m

Source: Produced by the author.

Note: Data available in Hoidalen, Prikler e Penaloza [2021]

4.1 Steady-state Evaluation

A scenario in which the EIBR is set to generate 1.025 MW with unitary power factor is considered in the first analysis, assuming that the current injection begins at $t = 0.02\ s$. Also, the alternative 1 for grid synchronization (LPF-PLL) is adopted, since this approach is the same as the reference model.

Under these circumstances, in Figure 21, it is possible to observe the phase A grid voltage with and without the generator. It is noticed that the grid voltage had no impact due to the presence of the generator by itself, since the graphical results are identical. This is the expected behavior from a grid-following IBR.

Figure 21 – Voltage in phase A with IBR connected and disconnected to the grid.

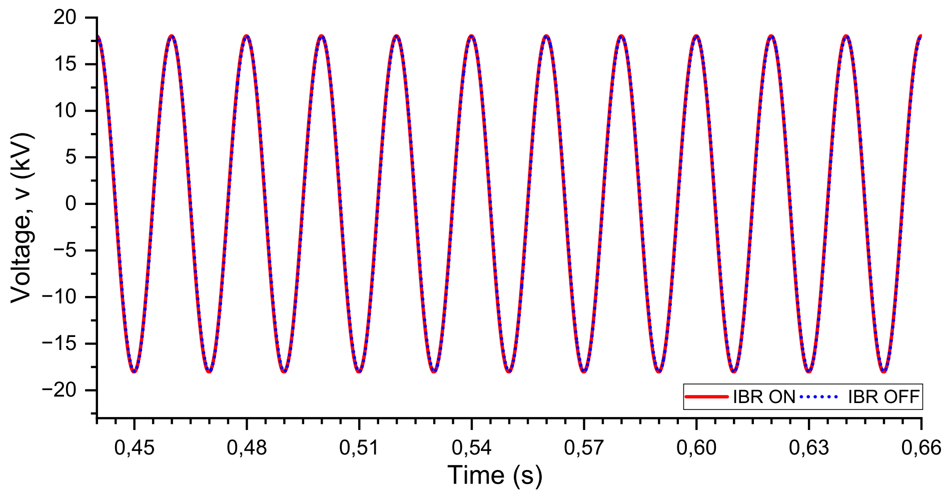

Source: Produced by the author

Following the analysis, Figure 22 presents phase A voltages and currents obtained from both proposed and reference models at the connecting point to the grid. It is noticed that the waveforms are very similar, except by the additional transients verified in the reference model due to the switching process, which is not included in the proposed EIBR.

Although the currents waveforms presented in Figure 22 are very similar, the mentioned differences can be observed if a zoom is applied, as shown in Figure 23.

Regarding the injected active power, the comparison results indicate a root mean squared error (RMSE) in the apparent power of 2.3184 kVA (about 0.23 % of the expected value).

Attested the suitability of the model considering steady-state operation, the next step is the analysis during grid disturbances.

Figure 22 – Comparison between the reference and proposed models in steady-state

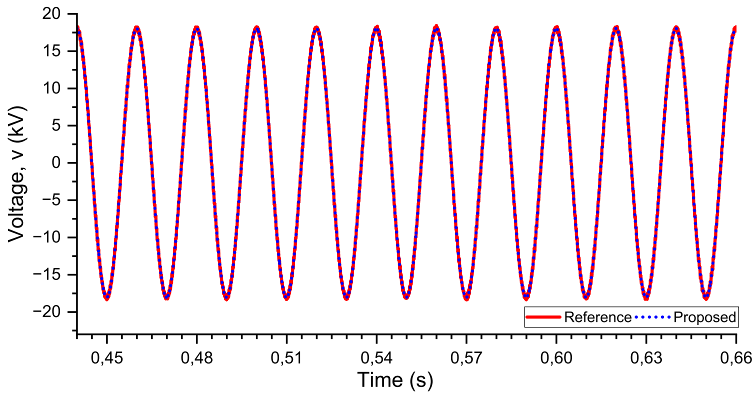

(a) Voltage in phase A

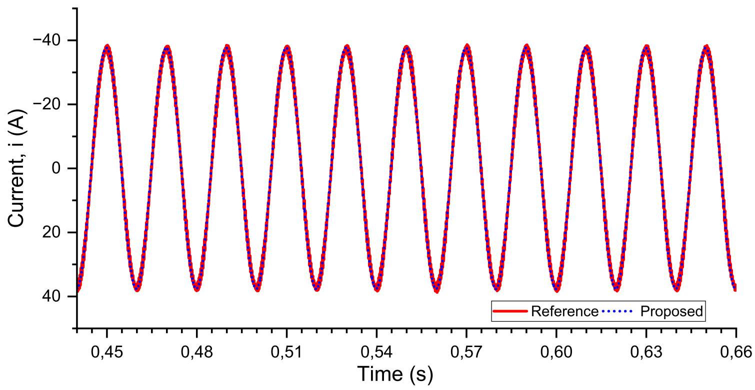

(b) Current in phase A

Source: Produced by the author

Figure 23 – Detailed current in phase A.

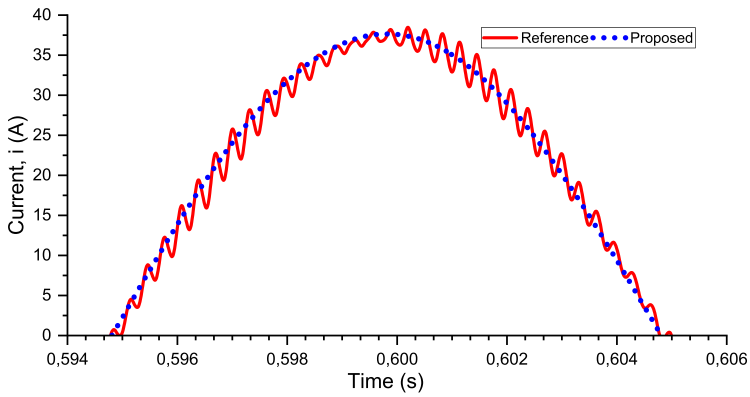

Source: Produced by the author

4.2 Fault Condition

To verify the behavior of the proposed model in cases of faults on the interconnecting grid, three scenarios are analyzed, namely: three-phase (3Ph), line-to-line (LL) and single-line-to-ground (SLG) short-circuits. One at a time, these faults were applied to the system.

In all cases, the fault duration was set to be 0.10 s (from $t = 0.45$ to $t = 0.55$ s), being the fault resistance set as $R_{fault} = 5\ \Omega$ and located in the middle on the line.

4.2.1 Grid Synchronization

Aiming to verify the performance of PLL under a faulty condition, the grid synchronization will be evaluated in this section. For this analysis, Figure 24 shows grid voltage and $cos(\theta + \omega \cdot t)$ extracted from both reference and proposed models during a 3Ph fault. Concerning the proposed model, the LPF-PLL implementation is considered at this point, as in the reference.

Figure 24 – Phase A voltage and $cos(\theta + \omega \cdot t)$ during a 3Ph grid fault

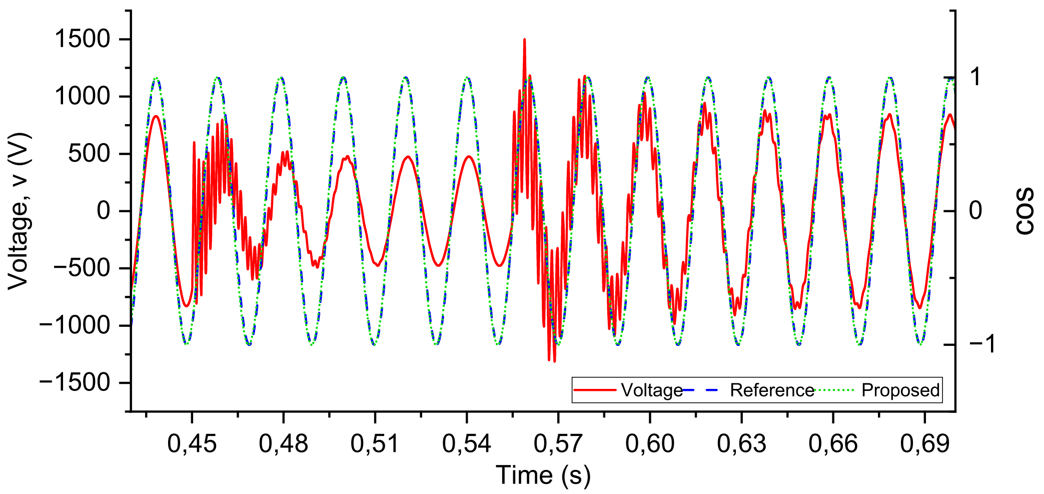

Source: Produced by the author

As it can be seen, both models perform very similarly. However, they are not very accurate during the beginning and clearing of the fault, which was not observed in the steady-state analysis (Figure 19). This deviation will be discussed in the next sections.

4.2.2 Power Injection

To analyze the first scenario, voltages in phase A, B and C and current in phase A obtained in the point of connection (POC) from the reference IBR and proposed EIBR model under 3Ph fault conditions are shown in Figures 25, 26, 27 and 28, respectively. Since the current synthesis process adopted in this work guarantee that they are balanced, only one phase current is presented in this dissertation. Again, the obtained results are very similar, except by some transients which are not verified in the simplified proposed EIBR. It is worth mentioning that, as commented in section 2, the analyzed IBR output currents are limited to values very close to those observed during the steady-state, even if faults take place on the interconnecting system. Here, such a limiting level is equal to 1.02 pu of the steady-state current, resulting in 843.5 A in the analyzed system.

Figure 25 – Phase A voltages during a 3Ph grid fault

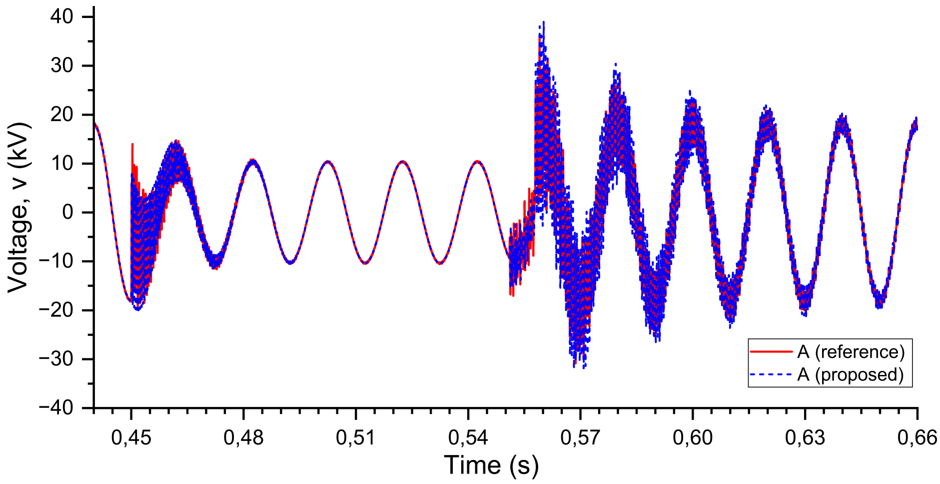

Source: Produced by the author

Figure 26 – Phase B voltages during a 3Ph grid fault

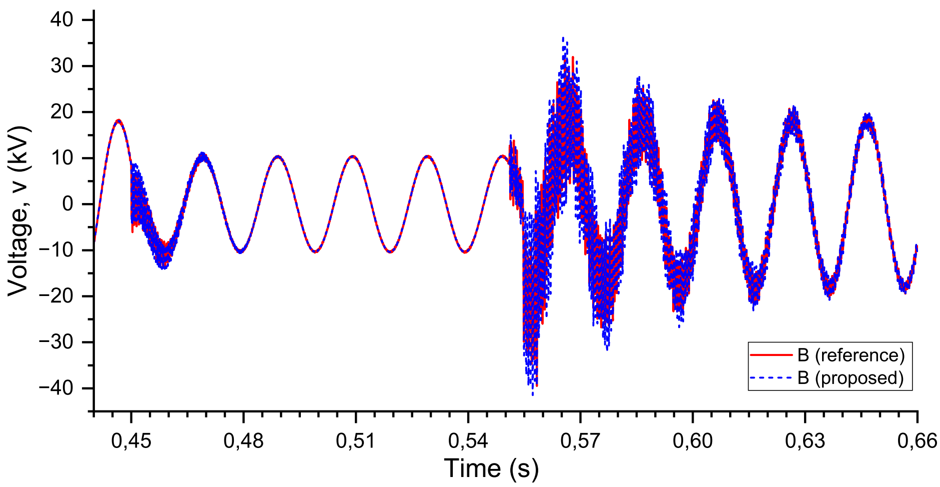

Source: Produced by the author

Figure 27 – Phase C voltages during a 3Ph grid fault

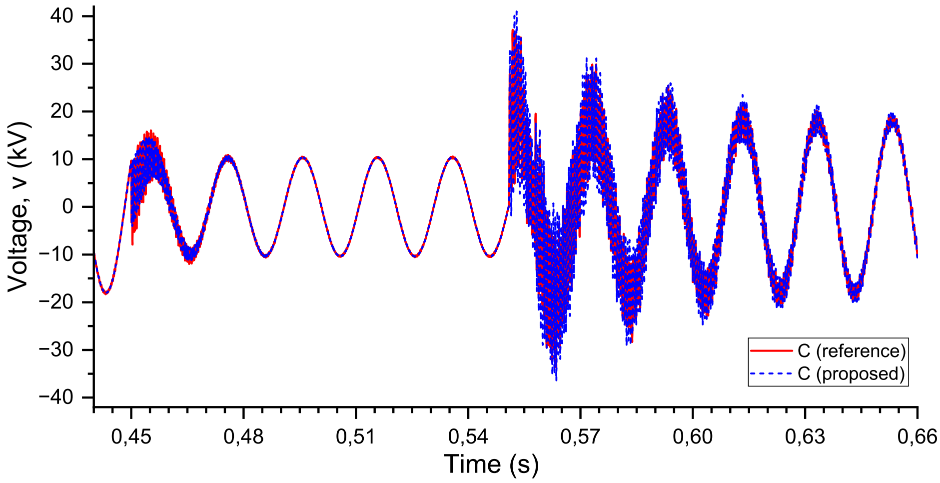

Source: Produced by the author

Figure 28 – Current injected in phase A during a 3Ph grid fault

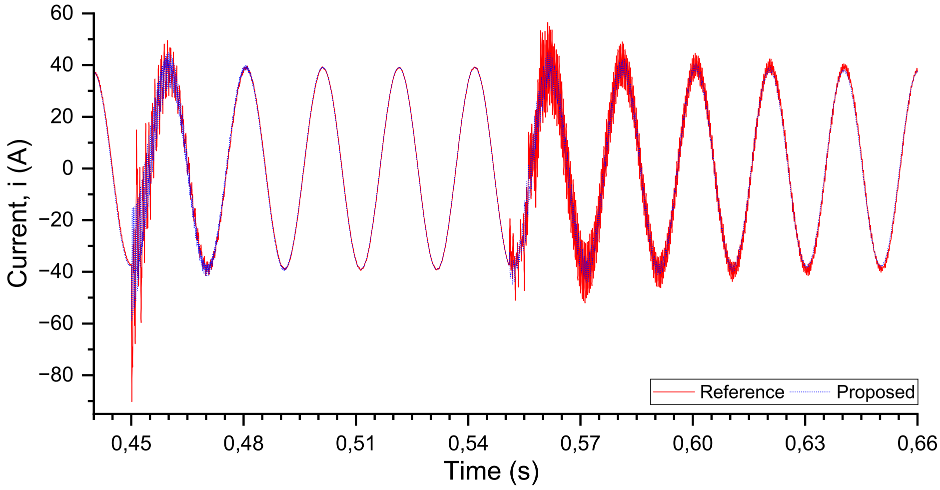

Source: Produced by the author

In order to provide a accurate comparison of the reference and proposed models, Figure 29 presents in details the voltage transients during the clearing of the fault (the most severe moment of the simulation). It is possible to observe that they have similar transient behavior during this critical moment for the system. Since there are no major differences in the other phases, this analysis will be restricted to phase A.

Figure 29 – Detailed phase A voltages during a 3Ph grid fault

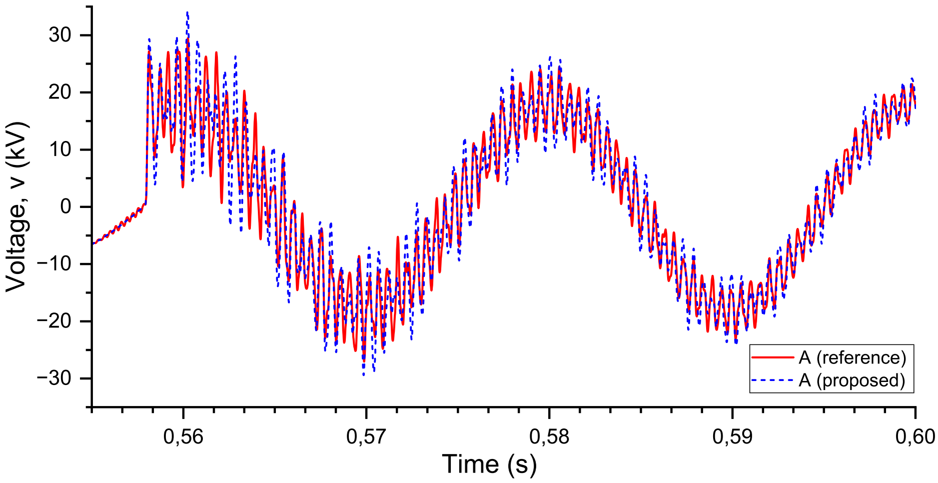

Source: Produced by the author

In addition, Figure 30 depicts the active and reactive powers injected into the grid during the fault. The presented comparison points out that both models are very close between each other, resulting in a value of root mean squared error (RMSE) in the active and reactive power equal to 30.878 kW and 23.233 kvar, respectively, and for the apparent power equal to 29.978 kVA (about 3.09% of the expected power).

Figure 30 – Power injected during a 3Ph fault

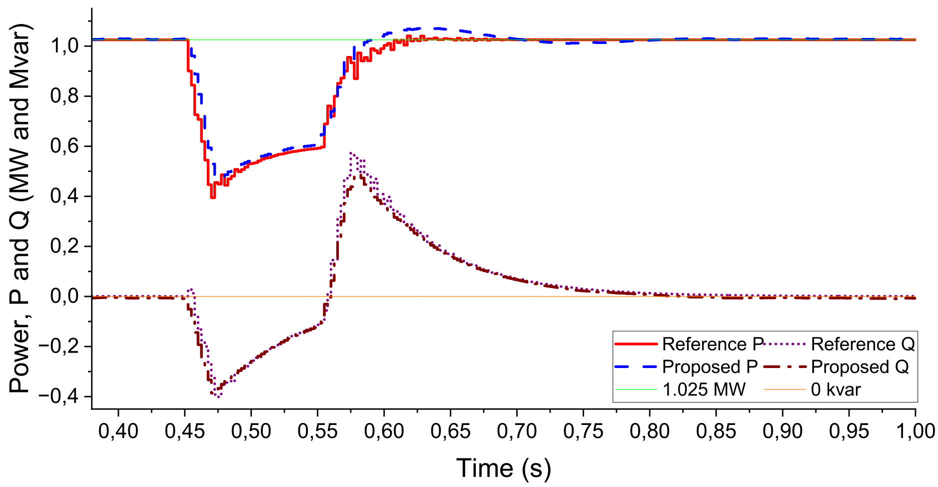

Source: Produced by the author

In the second analyzed case, a SLG fault on phase A is simulated. Figures 31, 32, 33 and 34 presents, respectively, the comparison between the voltages in phase A, B, C and current injected into the grid in phase A, both obtained via reference and proposed models. As the transient behavior during the clearing of the fault is similar to the last case, the detailed waveforms will not be explored in this case or in the next one.

In addition, Figure 35 compares the related active and reactive powers.

Figure 31 – Phase A voltages during a SLG grid fault

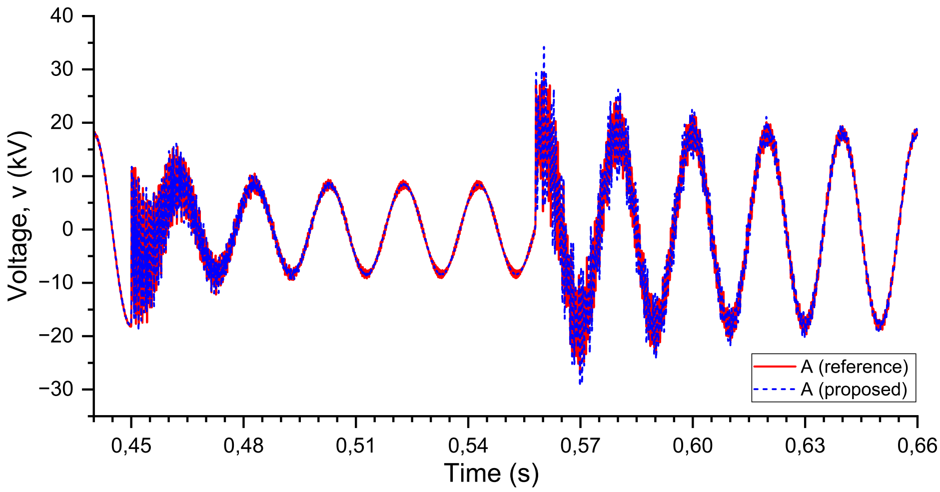

Source: Produced by the author

Figure 32 – Phase B voltages during a SLG grid fault

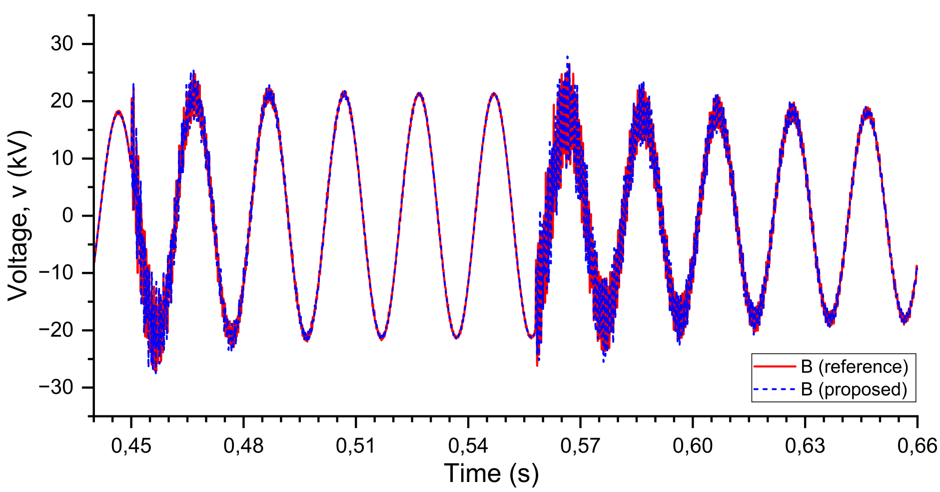

Source: Produced by the author

Figure 33 – Phase C voltages during a SLG grid fault

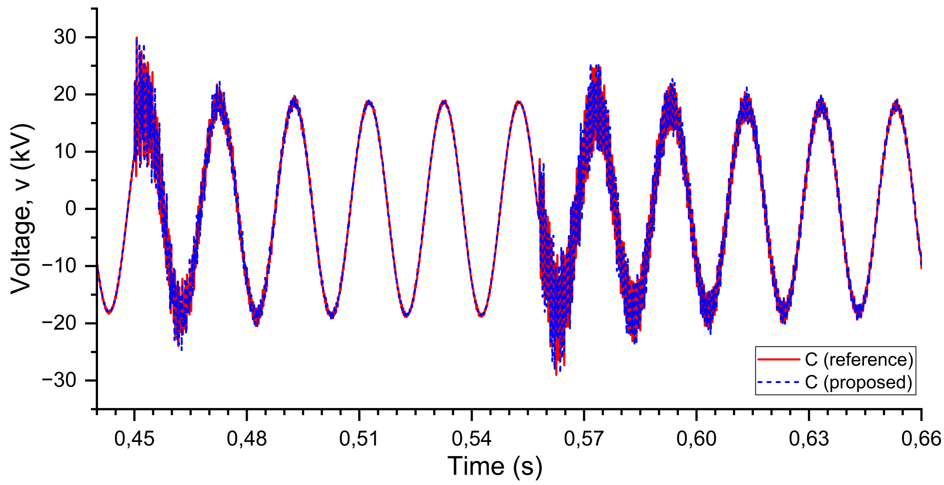

Source: Produced by the author

Figure 34 – Current injected in phase A during a SLG grid fault

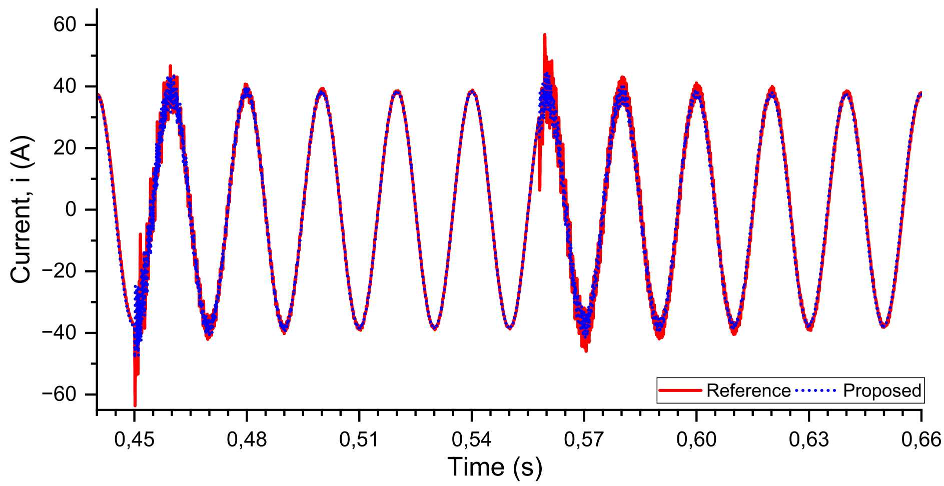

Source: Produced by the author

Similarly to the first case, only slight differences are observed in the obtained results, which are majorly related to transients caused by the inverter operation, which are not represented in the proposed simplified EIBR model. Indeed, from the comparison carried out, the RMSE for P and Q is equal to 21.538 kW and 13.432 kvar, respectively. Concerning the apparent power error, the value is 21.358 kVA, i.e., about only 2.12% of the expected value.

Figure 35 – Injected power during a SLG fault

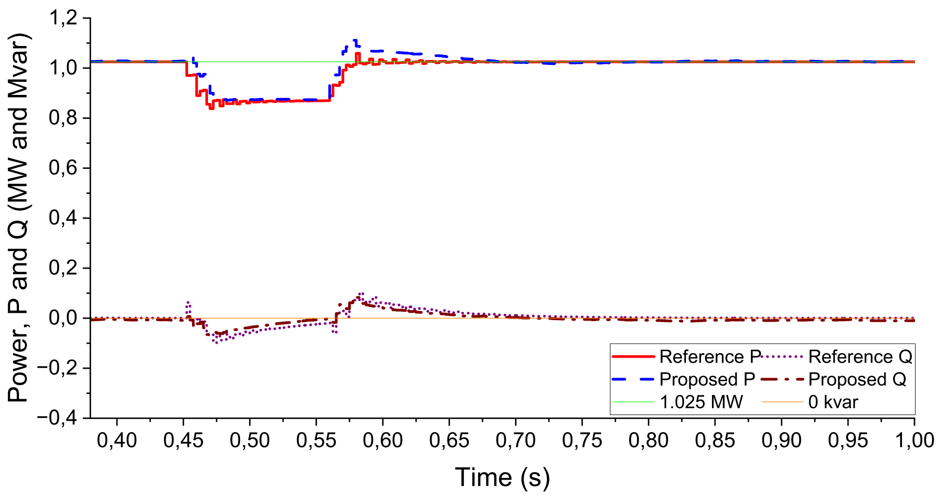

Source: Produced by the author

The last fault case consists of a LL fault between phases A and C. Figures 36, 37 and 38 shows the phase A, B and C voltages, respectively, at the POC for this case. The IBR output currents injected in phase A and the active and reactive powers injected into the grid are shown in Figure 39 and Figure 40, respectively, comparing again the results obtained from both reference and proposed models.

Figure 36 – Phase A voltages during an LL grid fault

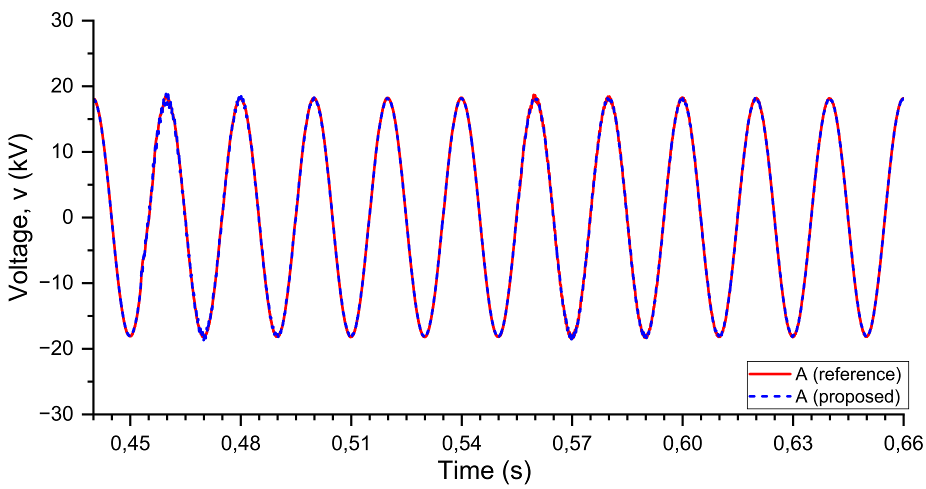

Source: Produced by the author

Figure 37 – Phase B voltages during an LL grid fault

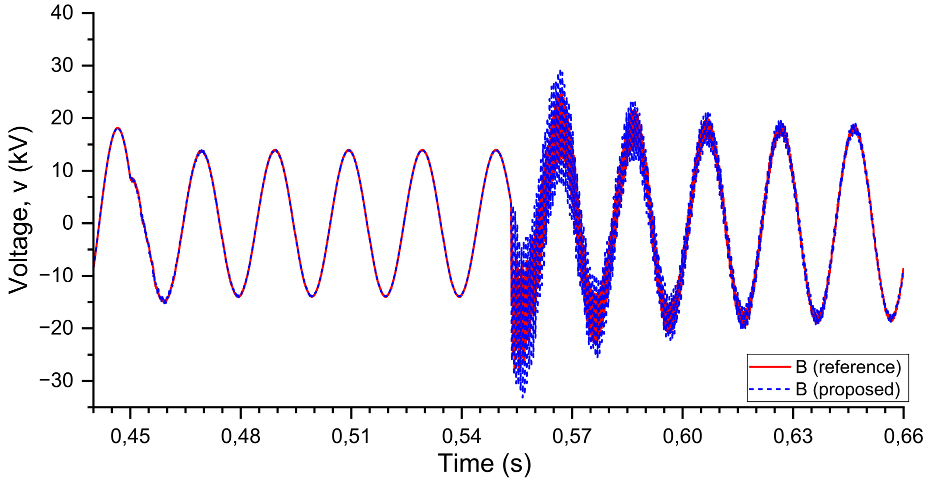

Source: Produced by the author

Figure 38 – Phase C voltages during an LL grid fault

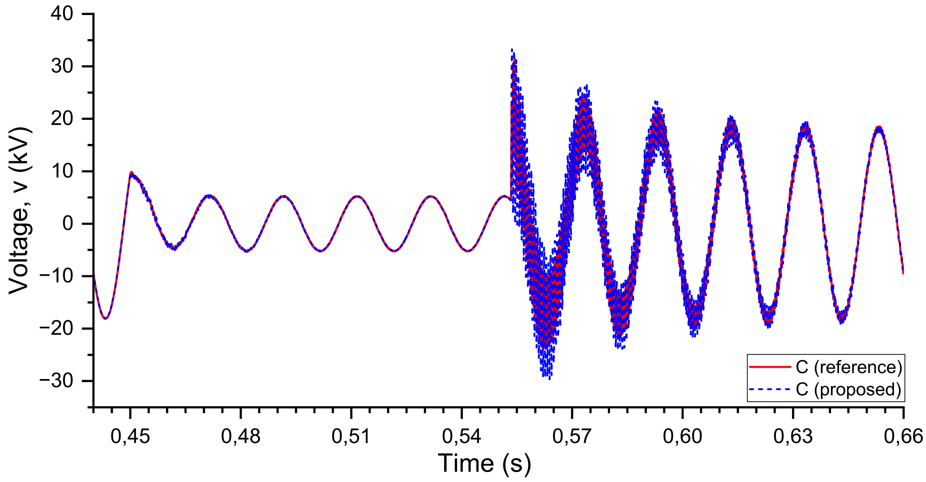

Source: Produced by the author

Once more, the most relevant discrepancy between the obtained waveforms regards to transients caused by the inverters, which are fully represented in the reference model, but disregarded in the proposed EIBR, for the sake of simplification. These transients have some slight impact in the power delivered to the grid, but it does not compromise the IBR dynamic representation.

Figure 39 – Current injected in phase A during an LL grid fault

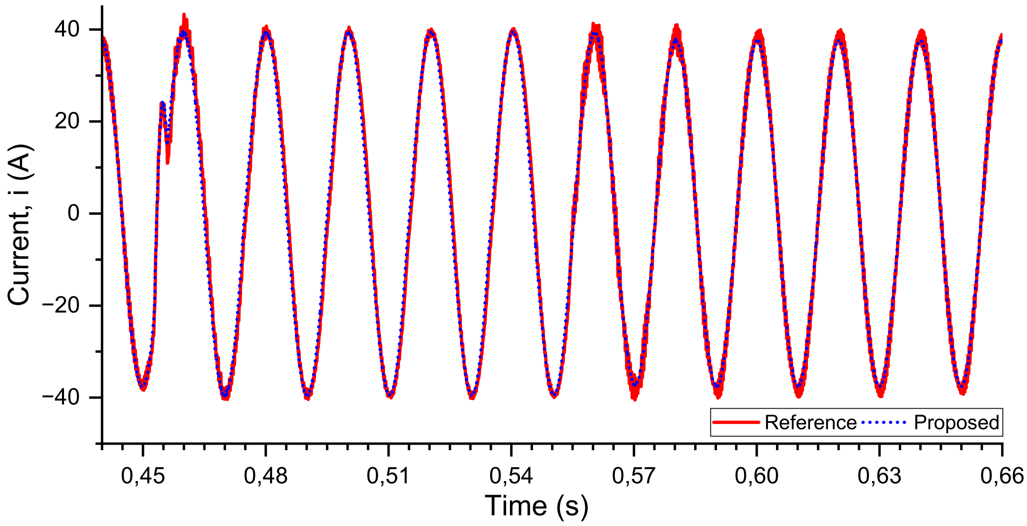

Source: Produced by the author

Figure 40 – Injected power during a LL fault

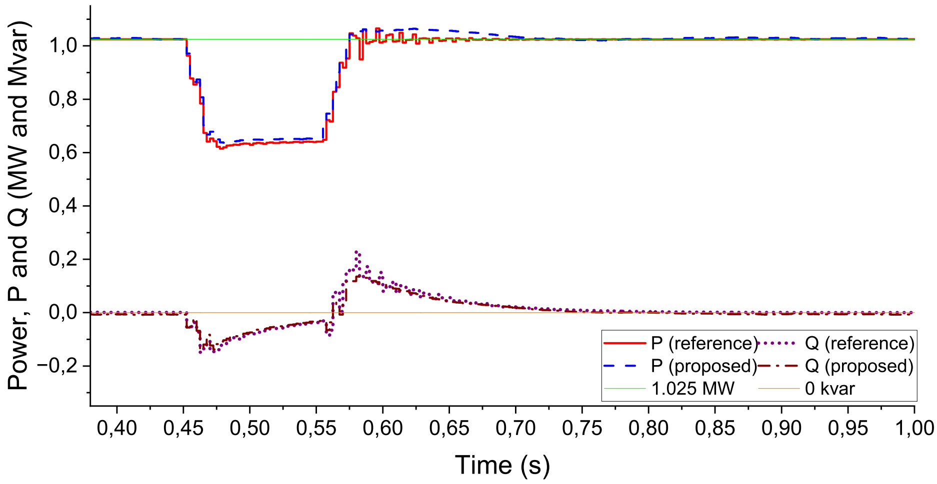

Source: Produced by the author

Indeed, the behavior of the proposed model showed again to be accurate and reliable, resulting in a RMSE for P and Q equal to 17.856 kW and 12.722 kvar, respectively, which results in a RMSE of 17.246 kVA for the apparent power, representing 1.77% of the expected power.

The presented results demonstrate that the proposed EIBR is quite reliable and accurate to represent the IBR operation during both steady-state and fault conditions, especially for EMTP studies focused on the fundamental frequency component. However, besides the accuracy, the associated computational burden is an important aspect, which must be assessed. Thus, the simulation times for both reference full IBR model and proposed simplified EIBR model were compared for a simulation of 1 s. The obtained results revealed that the proposed model demanded about 70% less time than the original one, since the reference model simulation took 60 s and the proposed model took 19 s, which demonstrates the suitability of the proposed model for EMTP IBR studies. A laptop with Intel Core i7 Processor (2.7 GHz) and 8 GB DDR4 RAM was used to run the simulations.

The RMSE results for the apparent power on each scenario are summarized in Table 4.

Table 4 – Apparent power RMSE for each scenario.

Scenario	RMSE
Steady-state	2.3184 kVA (0.23 %)
3Ph	29.978 kVA (3.09 %)
SLG	21.358 kVA (2.12 %)
LL	17.246 kVA (1.77 %)
Standard fault cases average	2.33

Source: Produced by the author.

4.2.3 Variations of grid fault characteristics

In order to carry out a detailed evaluation of the proposed EIBR model under different operational conditions, some variations in the characteristics of the short-circuits analyzed in the previous section were explored and the system response is here presented. The modifications includes: fault resistance, fault location and incidence angle of the fault.

4.2.3.1 Fault resistance

The resistance of the fault applied in the simulations was varied and the performance of the model was verified.

In these analyses, three different versions of the SLG and LL short-circuits were considered for $R_{fault} = 10, 25$ and 60 Ω.

The RMSE of the apparent power in the above mentioned cases is summarized in Table 5.

Table 5 – Apparent power RMSE for each fault resistance scenario.

R_{fault}	SLG fault	LL fault
10 Ω	19.545 kVA (1.91 %)	31.601 kVA (3.2 %)
25 Ω	14.165 kVA (1.38 %)	23.498 kVA (2.3 %)
60 Ω	4.159 kVA (0.41 %)	15.056 kVA (1.47 %)
Average	1.23 %	2.32 %

Source: Produced by the author.

The results showed the consistency of the model under different short-circuit resistances, with a average error of 1.775%. It can be observed a tendency for the error to decrease as the fault resistance increases due to the fact that it results in least severe conditions to the system concerning the voltage swag caused by the fault.

4.2.3.2 Fault location

To assess the behavior of the model with regard to the location of the fault, the LL and 3Ph short-circuits were applied at two different points of the transmission line: at 1/3 and at 2/3 of its total length. The results are presented in Table 6.

Table 6 – Apparent power RMSE for each fault location scenario.

.

Location	LL fault	3ph fault
1/3	17.239 kVA (1.72 %)	22.843 kVA (2.3 %)
2/3	21.907 kVA (2.26 %)	25.758 kVA (2.69 %)
Average	1.99 %	2.495 %

Source: Produced by the author.

Considering the results, the model is capable of representing grid faults at different locations of the line with accuracy, with an average RMSE of 2.253%.

4.2.3.3 Incidence angle of the fault

In this section, different incidence angles of the SLG and LL short-circuits were evaluated. Three angles were considered: $0^o, 45^o$ and 90^o, taking phase A as reference. The obtained results are summarized in Table 7.

In these last scenarios, the model showed to remain adequate for the analyses, with an average error of 2.49%. The results indicate that the incidence angle of 90^o is the most critical one, in which the largest errors were observed for both SLG and LL faults.

Table 7 – Apparent power RMSE for each fault angle of incidence scenario.

Incidence angle	SLG fault	LL fault
0^o	16.604 kVA (1.65 %)	21.529 kVA (2.22 %)
45^o	21.310 kVA (2.11 %)	21.045 kVA (2.16 %)
90^o	28.764 kVA (2.85 %)	38.741 kVA (3.97 %)
Average	2.2 %	2.78 %

Source: Produced by the author.

4.3 Evaluation of the EIBR model capabilities

The proposed EIBR model is designed to be adaptable regarding the implementation of different control strategies or different IBR components. Thus, this section evaluates the performance of the model demonstrating the application of different design scenarios.

4.3.1 Alternative GS method

Initially, grid synchronization alternative 2, i.e., DSOGI-PLL is considered rather than the LPF-PLL. The 3Ph fault scenario is evaluated again, being the results in terms of power shown in Figure 41.

Figure 41 – Injected power during a 3Ph fault using the DSOGI-PLL

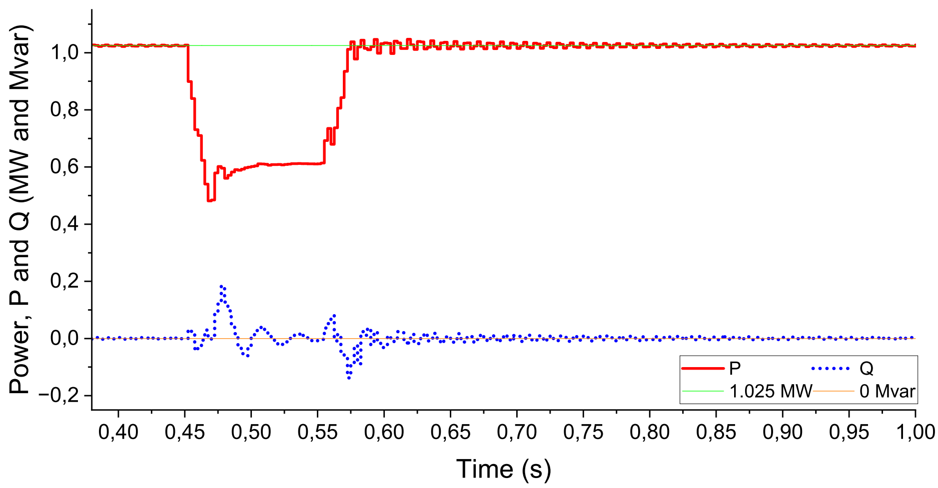

Source: Produced by the author

It can be seen that, from straightforward adaptations, the proposed model was properly prepared to utilize a different grid synchronization approach (moreover, current synthesis, control strategies etc). The results remained consistent, revealing that the second

PLL alternative has a better performance during system transients, as shown in Figure 42, resulting in less deviations in relation to the reference value.

Figure 42 – Phase A voltage and $cos(\theta + \omega \cdot t)$ with DSOGI-PLL

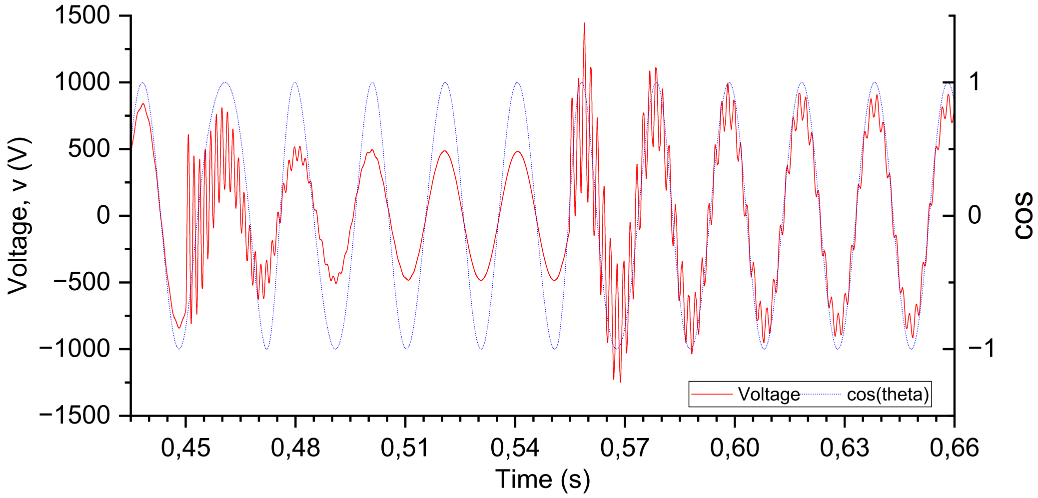

Source: Produced by the author

This improvement is evidenced when Figure 24 is observed and compared to the results presented in this section (Figure 42).

4.3.2 Reactive power injection

Since reactive power injection is a frequent requirement in grid codes worldwide, the capacity of the proposed EIBR model in performing this ancillary service is tested in both steady-state and faulty condition. For the first case, simulations were carried out in steady state considering a varying reactive power reference setting, which varies from 0 to 200 kvar at $t = 0.5$ s and from 200 to 500 kvar at $t = 0.7$ s. The obtained results are presented in Figure 43 and they demonstrate that the proposed EIBR model properly responds to such a type of setting.

In a second scenario, the reactive power injection capability is assessed under a SLG short-circuit in phase A, considering the original PLL implementation (LPF-PLL). In this case, the injected power values were defined in order to obtain a power factor of 0.9. The results are presented in Figure 44. It is possible to observe the adequacy of the model in representing reactive power injection even under faulty conditions.

Figure 43 – Reactive power injection capability in steady-state

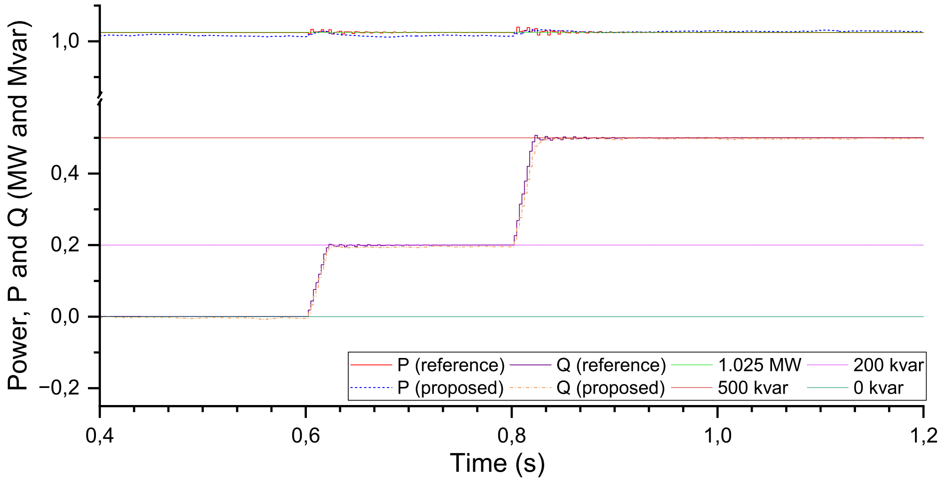

Source: Produced by the author

Figure 44 – Reactive power injection capability during a SLG fault

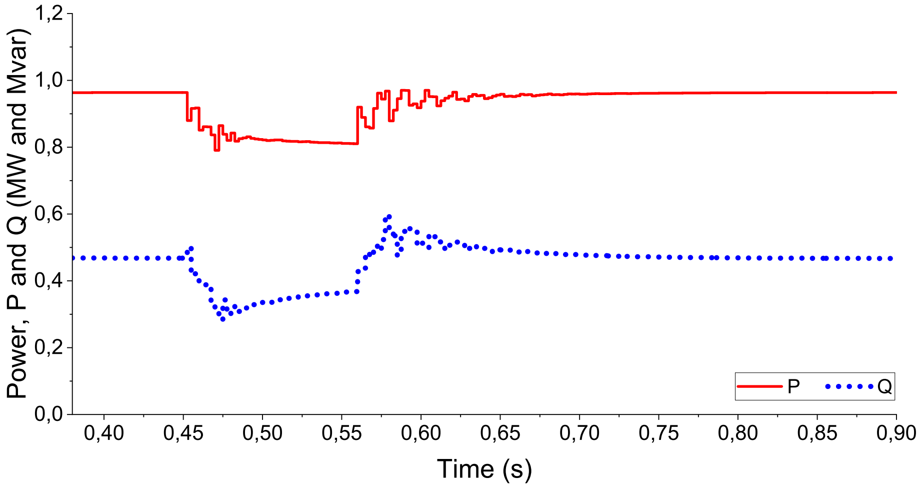

Source: Produced by the author

4.4 Final remarks

From the presented results, the proposed EIBR model proved to be an alternative to the full switched ones, being accurate in the representation of the electrical quantities usually analyzed in pre-operational and operational EPS studies in steady-state and under fault conditions, considering variations in the faults characteristics. The maximum RMSE obtained for the injected apparent power was 3.97 % (2.21 % on average, as stated in Table 8).

Table 8 – Average apparent power RMSE during a fault.

Scenario	RMSE (%)
Standard fault scenarios	2.33
Fault resistance variation	1.775
Fault location variation	2.243
Fault incidence angle variation	2.49
Average	**2.21**

Source: Produced by the author.

Also, it showed to be capable of considering the adoption of different elements implementations and settings of injected active and reactive power in steady-state and under faulty conditions. The simplicity of the proposed model resulted in a reduction of 70 % in the simulation time when compared to the reference model.

5 Conclusion and Future Work

5.1 Conclusion

This work presented the development of a simplified equivalent grid-following IBR model in ATP/ATPDraw platform. The software implementation was meticulously detailed to ensure its reproduction by other researchers. All elements necessary for the correct operation of the model were described, including two version of the PLL and the codes related to adopted transforms and current injection. This fills a gap in the existing literature since there is a shortage of works with this level of detail.

The model showed to be reliable and accurate in the representation of the fundamental frequency component in both steady-state and fault scenarios. Concerning these faulty conditions, the proposed implementation has successfully performed during single-line-to-ground, line-to-line and three-phase short-circuits. These short-circuits had their characteristics modified, which included the resistance, location and incidence angle of the fault. Deviations found in relation to a full IBR reference model were of about 2.21 % in the apparent power, providing also a very satisfactory representation of IBR output currents. Moreover, the proposed EIBR showed to be capable of performing ancillary services as reactive power injection (in steady-state and during a fault), responding adequately to the reference set for multiple reactive power values, which opens space for different applications of the model in future works.

The proposed EIBR model also showed to be flexible in terms of applying different control strategies and different settings of injected active and reactive, with the advantage of reducing by 70 % the simulation time in comparison to the analyzed complete IBR reference model. These results demonstrate that the proposed model is quite useful for IBR integration studies focused on the fundamental frequency component, especially if high IBR penetration scenarios are of interest.

Implementing models which have to represent accurately components with dynamic behavior is always a complex task. During the development of this work, some components (PLL, DSOGI, for example), had to be adapted in order to achieve better results when subjected to disturbances that are common in electrical systems.

5.2 Future works

The next steps of this research in order to continue and improve the model and the methodology are:

- Apply the model in a larger transmission system in order to verify the impacts of this connection, mainly during a fault or any other kind of disturbances;
- Expand the methodology considering different characteristics of electrical power systems, as load variation, intermittence of solar and wind powers etc;
- Utilize other control strategies in order to consider specific grid codes requirements;
- Expand the methodology to consider detailed fault ride-through (FRT) specificities; and
- Consider negative-sequence current injection;

Bibliography

[1] National Academies of Sciences Engineering & Medicine. *Analytic Research Foundations for the Next-Generation Electric Grid*. Washington, DC: The National Academies Press, 2016. ISBN 978-0-309-39231-0. Disponível em: <https://nap.nationalacademies.org/catalog/21919/analytic-research-foundations-for-the-next-generation-electric-grid>. Cited 2 times on pages 17 and 19.

[2] International Energy Agency. Share of cumulative power capacity by technology, 2010-2027. *Renewables 2022*, 2022. Cited on page 17.

[3] LOPES, F. V. et al. Importance of EMT-type simulations for protection studies in power systems with inverter-based resources. In: *2022 Workshop on Communication Networks and Power Systems (WCNPS)*. [S.l.: s.n.], 2022. p. 1–6. Cited 2 times on pages 18 and 34.

[4] KROPOSKI, B. et al. Achieving a 100% renewable grid: Operating electric power systems with extremely high levels of variable renewable energy. *IEEE Power and Energy Magazine*, v. 15, n. 2, p. 61–73, 2017. Cited 2 times on pages 18 and 19.

[5] MOHAMMED, N.; ALHELOU, H. H.; BAHRANI, B. E. *Grid-Forming Power Inverters: Control and Applications*. 1st edition. ed. [S.l.]: CRC Press, 2023. ISBN 9781003302520. Cited 4 times on pages 19, 20, 23, and 24.

[6] Copernicus Climate Change Service. July 2023: Global air and ocean temperatures reach new record highs. *European Centre for Medium-Range Weather Forecasts*, 2023. Cited on page 19.

[7] CORPORATION, N. A. E. R. Distributed energy resources connection modeling and reliability considerations. *Technical Report*, 2017. Cited 2 times on pages 19 and 25.

[8] MENDES, M. et al. Simplified single-phase pv generator model for distribution feeders with high penetration of power electronics-based systems. In: *15th IEEE Brazilian Power Electronics Conf. and 5th IEEE Southern Power Electronics Conf.* [S.l.: s.n.], 2019. p. 1–7. Cited 2 times on pages 19 and 26.

[9] HASSANI, R. et al. Evaluation of time-domain and phasor-domain methods for power system transients. *Electric Power Systems Research*, Elsevier, v. 212, p. 108335, 2022. Cited 2 times on pages 19 and 25.

[10] HWANG, P.-I. et al. Three-phase steady-state models for a distributed generator interfaced via a current-controlled voltage-source converter. *IEEE Transactions on Smart Grid*, v. 7, n. 3, p. 1694–1702, 2016. Cited 2 times on pages 19 and 26.

[11] POLAJžER, B. et al. Steady-state response of inverter-interfaced distributed generations during transmission network faults. In: *IEEE Intern. Conf. on Environment and Electrical Engineering and IEEE Industrial and Commercial Power Systems Europe*. [S.l.: s.n.], 2021. p. 1–6. Cited 2 times on pages 19 and 26.

[12] QUEIROZ, L. G. O.; MENDES, M. A.; BATISTA, O. E. Simplified dynamic pv generator model for analysis of voltage and current variation in feeder with high dg integration. In: *International Conf. on Electrical, Computer, Communications and Mechatronics Engineering*. [S.l.: s.n.], 2021. p. 1–6. Cited 2 times on pages 19 and 26.

[13] RAMASUBRAMANIAN, D. et al. Converter model for representing converter interfaced generation in large scale grid simulations. *IEEE Transactions on Power Systems*, v. 32, n. 1, p. 765–773, 2017. Cited 2 times on pages 20 and 26.

[14] LOPES, F. V. et al. Modelagem de fonte de potência controlada no ATP/ATPDraw: Um desenvolvimento alternativo para estudos de fluxo de potência. In: *Simpósio Brasileiro de Sistemas Elétricos*. [S.l.: s.n.], 2022. v. 2, n. 1. Cited 3 times on pages 20, 22, and 27.

[15] ROCABERT, J. et al. Control of power converters in ac microgrids. *IEEE Transactions on Power Electronics*, v. 27, n. 11, p. 4734–4749, 2012. Cited 3 times on pages 23, 24, and 28.

[16] BIALASIEWICZ, J. T. Renewable energy systems with photovoltaic power generators: Operation and modeling. *IEEE Transactions on Industrial Electronics*, v. 55, n. 7, p. 2752–2758, 2008. Cited on page 23.

[17] VASQUEZ, J. C. et al. Adaptive droop control applied to voltage-source inverters operating in grid-connected and islanded modes. *IEEE Transactions on Industrial Electronics*, v. 56, n. 10, p. 4088–4096, 2009. Cited on page 25.

[18] REICHERT, S.; GRIEPENTROG, G.; STICKAN, B. Comparison between grid-feeding and grid-supporting inverters regarding power quality. In: *2017 IEEE 8th International Symposium on Power Electronics for Distributed Generation Systems (PEDG)*. [S.l.: s.n.], 2017. p. 1–4. Cited on page 25.

[19] ROPP, M. E.; GONZALEZ, S. Development of a matlab/simulink model of a single-phase grid-connected photovoltaic system. *IEEE Transactions on Energy Conversion*, v. 24, n. 1, p. 195–202, 2009. Cited on page 25.

[20] SEUSS, J. et al. *Determining the Impact of Steady-State PV Fault Current Injections on Distribution Protection*. [S.l.], 2017. Disponível em: <https://www.osti.gov/biblio/1367427>. Cited on page 25.

[21] DASH, P. P.; KAZERANI, M. Dynamic modeling and performance analysis of a grid-connected current-source inverter-based photovoltaic system. *IEEE Transactions on Sustainable Energy*, v. 2, n. 4, p. 443–450, 2011. Cited on page 25.

[22] DONGDONG, L. et al. Design and implementation of space vector modulated three phase voltage source inverter. In: *2019 IEEE International Conference on Sustainable Energy Technologies and Systems (ICSETS)*. [S.l.: s.n.], 2019. p. 331–335. Cited on page 25.

[23] NANOU, S. I.; PAPATHANASSIOU, S. A. Modeling of a pv system with grid code compatibility. *Electric Power Systems Research*, v. 116, p. 301–310, 2014. ISSN 0378-7796. Cited on page 25.

[24] SARMIENTO, J. E.; CARRENO, E. M.; Z. de S. A. C. Modeling inverters with volt-var functions in grid-connected mode and droop control method in islanded mode. *Electric Power Systems Research*, v. 155, p. 265–273, 2018. ISSN 0378-7796. Cited on page 27.

[25] TURNER-BANDELE, N.; PANDEY, A.; PILEGGI, L. Analytical inverter-based distributed generator model for power flow analysis. In: *2021 IEEE Power Energy Society General Meeting (PESGM)*. [S.l.: s.n.], 2021. p. 1–5. Cited on page 27.

[26] GUI, Y. et al. Voltage-modulated direct power control for a weak grid-connected voltage source inverters. *IEEE Transactions on Power Electronics*, v. 34, n. 11, p. 11383–11395, 2019. Cited on page 27.

[27] HOIDALEN, H. K.; PRIKLER, L.; PENALOZA, F. Atpdraw version 7.3 for windows. *User's Manual*, 2021. Cited 6 times on pages 27, 34, 35, 36, 41, and 45.

[28] KAURA, V.; BLASKO, V. Operation of a phase locked loop system under distorted utility conditions. *IEEE Transactions on Industry Applications*, v. 33, n. 1, p. 58–63, 1997. Cited on page 29.

[29] RODRíGUEZ, P. et al. New positive-sequence voltage detector for grid synchronization of power converters under faulty grid conditions. In: *37th IEEE Power Electronics Specialists Conf.* [S.l.: s.n.], 2006. p. 1–7. Cited 3 times on pages 29, 30, and 41.

[30] ARINDAM, G.; AVINASH, J. A new algorithm for the generation of reference voltages of a dvr using the method of instantaneous symmetrical components. *IEEE Power Engineering Review*, v. 22, n. 1, p. 63–65, 2002. Cited on page 29.

[31] VINTON, W. L. Application of the method of symmetrical components. In: _____. [S.l.]: Mcgraw-hill Book Company Inc., New York and London, 1937. Cited on page 29.

[32] HUANG, T. et al. Three-phase photovoltaic grid-connected inverter based on feedforward decoupling control. In: *2013 International Conference on Materials for Renewable Energy and Environment*. [S.l.: s.n.], 2013. v. 2, p. 476–480. Cited on page 31.

[33] SUYATA, T.-I.; PO-NGAM, S. Simplified active power and reactive power control with mppt for three-phase grid-connected photovoltaic inverters. In: *2014 11th International Conference on Electrical Engineering/Electronics, Computer, Telecommunications and Information Technology (ECTI-CON)*. [S.l.: s.n.], 2014. p. 1–4. Cited on page 32.

[34] SATO, F.; FREITAS, W. *Análise de Curto- circuito e Princípios de Proteção em Sistemas de Energia Elétrica: Fundamentos e Prática*. Rio de Janeiro, RJ: GEN LTC, 2014. 472 p. ISBN 978-8535268867. Cited on page 33.

[35] LONG, W. et al. EMTP-a powerful tool for analyzing power system transients. *IEEE Computer Applications in Power*, v. 3, n. 3, p. 36–41, 1990. Cited on page 34.

[36] GIMENES, T. K. et al. Impact of distributed energy resources on power quality: Brazilian scenario analysis. *Electric Power Systems Research*, v. 211, p. 108249, 2022. ISSN 0378-7796. Disponível em: <https://www.sciencedirect.com/science/article/pii/S0378779622004527>. Cited on page 34.